

1-1-2017

Monte-Carlo Event Generators For Jet Modification In D(p)-A And A-A Collisions

Michael Charles Kordell Ii
Wayne State University,

Follow this and additional works at: https://digitalcommons.wayne.edu/oa_dissertations



Part of the [Nuclear Commons](#)

Recommended Citation

Kordell Ii, Michael Charles, "Monte-Carlo Event Generators For Jet Modification In D(p)-A And A-A Collisions" (2017). *Wayne State University Dissertations*. 1825.

https://digitalcommons.wayne.edu/oa_dissertations/1825

This Open Access Dissertation is brought to you for free and open access by DigitalCommons@WayneState. It has been accepted for inclusion in Wayne State University Dissertations by an authorized administrator of DigitalCommons@WayneState.

**MONTE-CARLO EVENT GENERATORS FOR JET MODIFICATION IN
d(p)-A AND A-A COLLISIONS**

by

MICHAEL C. KORDELL II

DISSERTATION

Submitted to the Graduate School

of Wayne State University,

Detroit, Michigan

in partial fulfillment of the requirements

for the degree of

DOCTOR OF PHILOSOPHY

2017

MAJOR: Physics

Approved By:

Advisor

© COPYRIGHT BY
MICHAEL C. KORDELL II
2017
All Rights Reserved

ACKNOWLEDGEMENTS

I would like to express my deep gratitude to my advisor Dr. Abhijit Majumder for his aid and support, without which this research would not have been possible. Also, Dr. Rainer Fries for his support and collaboration while hosting me at Texas A&M during the final phase of my doctoral research. I would also like to state my appreciation for my committee members, Dr. Justin Frantz, Dr. Sean Gavin, and Dr. Alexey Petrov for their mentoring and collaboration.

Further, I would like to thank Chathuranga, Shanshan, and Kolja for their helpful discussions. Additionally, I would like to thank Amit for his helpful discussions and for his hospitality.

This work would not have been possible without the funding provided by the NSF under grant number PHY-1207918, by the U.S. DOE under grant number DE-SC0013460, and by the Thomas Rumble Fellowship, for which I am thankful of their support.

I would also like to thank my family and friends, particularly Alex and Debbie for not only welcoming me into the family but providing a continual source of encouragement and support over the years. Finally, last but not least, I would like to express my heartfelt appreciation to Helen for holding down the home front throughout several cross country moves, late nights, and long trips in addition to her unwavering support and encouragement through thick and thin.

TABLE OF CONTENTS

Acknowledgments	ii
List of Figures	v
Chapter 1 Introduction	1
1.1 The Strong Force and Quantum Chromodynamics	1
1.2 Heavy-Ion Collisions and the Quark Gluon Plasma	4
1.3 Jets and Leading Hadrons	10
Chapter 2 Centrality Dependent Effects of Jet Production in $d(p)$-A Collisions	16
2.1 Introduction	16
2.2 Simulation Details	19
2.2.1 Sampling the nuclear distribution	19
2.2.1.1 The Deuteron:	19
2.2.1.2 The Large Nucleus (Au or Pb)	20
2.2.1.3 Transverse Size of Nucleons and Binary Collisions:	23
2.2.2 The Modified Parton Distribution Function	25
2.3 Results and Experimental Comparison	35
2.4 Discussion	50
Chapter 3 Event-by-Event Simulations of Jet Modification in A-A Collisions 53	
3.1 Introduction	53
3.2 Theory of Jet Energy Loss	54
3.3 Phenomenology of Jet Energy Loss	58
3.3.1 Generating the Initiating Hard Parton using PYTHIA	59
3.3.2 Hydrodynamic Simulation of the QGP	59
3.3.3 The MATTER Event Generator	61
3.4 Results and Experimental Comparison	64
3.4.1 Integration of the Texas A&M Recombination Code	66

3.5 Discussion	67
Chapter 4 Summary and Discussion	71
4.1 Summary	71
4.2 Discussion	73
Bibliography	76
Abstract	82
Autobiographical Statement	84

LIST OF FIGURES

Figure 1.1	Feynman diagrams of QED and QCD vertices; note that while both photons in QED and gluons in QCD couple to charged fermions, gluons can couple to gluons in contrast to photons which cannot couple to other photons.	2
Figure 1.2	An illustration of color confinement: the energy dumped into a system when attempting to remove a colored object from a colorless object results in the creation of a quark-antiquark pair causing the system to collapse into two colorless objects. Taken from http://webific.ific.uv.es/web/en/content/lattice-qcd-numerical-approach-strong-force	3
Figure 1.3	Visualizations of the composition of a proton with varying degrees of complexity.	4
Figure 1.4	Plots of the CTEQ6l [1] parton distribution function for a proton.	5
Figure 1.5	A plot of the elliptic flow v_2 at differing centralities for differing values of η/s ; taken from [2]. The experimental data in this plot are from STAR [3] and ALICE [4].	6
Figure 1.6	An illustration of the different stages of a heavy-ion collision. Taken from https://arxiv.org/pdf/1201.4264	6
Figure 1.7	An illustration showing non-interacting spectator nucleons escaping the collision and the creation of a colored QGP from the participant nucleons. Taken from http://alicematters.web.cern.ch/?q=town_meeting_062012	7
Figure 1.8	A phase diagram for states of matter constrained by QCD. Taken from https://science.energy.gov/~media/np/nsac/pdf/2015LRP/2015_LRPNS_091815.pdf	7
Figure 1.9	A diagram of a dijet event where one jet has significant interaction with the medium. Taken from https://arxiv.org/pdf/0902.2011	11
Figure 2.1	The sampled Hulthén distribution for two nucleons in a deuteron.	20
Figure 2.2	The sampled Woods-Saxon distribution for a large nucleus (in this case Au with an $A = 192$.)	21
Figure 2.3	Three separate events in d - Au collisions. Nucleon distributions are projected onto the x - y plane.	22

Figure 2.4	The event distribution in d - Au collisions as a function of the number of binary collisions and the division of events in the four different centrality bins.	25
Figure 2.5	The multiplicity of charged particles in a simulated d - Au collision with the Au side simulated as a super-nucleon with a parton distribution function given as $F_S(x) = n_p F_p(x) + n_n F_n(x)$, and energy enhanced as $E_S = (n_p + n_n)E$. In the above plot $n_p = 10$, and $n_n = 10$	27
Figure 2.6	The pseudo-rapidity distribution of charged particles in a simulated d - Au collision with the Au side simulated as a super-nucleon with a parton distribution function given as $F_S(x) = n_p F_p(x) + n_n F_n(x)$, and energy enhanced as $E_S = (n_p + n_n)E$	28
Figure 2.7	The ratio of the gluon distribution in a super-nucleon to that in a nucleon as a function of x , the energy fraction of the gluon, relative to the projectile nucleon.	29
Figure 2.8	The ratio of the shadowed gluon distribution in a super nucleon to that in a regular nucleon as a function of the number of collisions N_{coll} (See Eq. (2.4)). The normalization of each line is adjusted to reflect the function that is sampled by the PYTHIA event generator, which continues to sample distributions until the momentum of the nucleon is exhausted.	31
Figure 2.9	The distribution of charged particles produced in a p - Pb collision, as a function of the number of collisions suffered by the projectile proton.	33
Figure 2.10	The distribution of the number of charged particles produced and the division of the events in the four different centrality bins.	33
Figure 2.11	The nuclear modification factor for neutral pions for minimum bias d - Au collisions at RHIC. Experimental data are taken from Ref. [5]	35
Figure 2.12	The nuclear modification factor for neutral pions for 0 - 20% most central d - Au collisions at RHIC. The simulation is carried out by binning in centrality according to the number of binary collisions (prescription A: see text for details). Simulations include shadowing and no energy loss. Experimental data are taken from Ref. [5]	36
Figure 2.13	Same as Fig. 2.12, except for 20-40% centrality.	37
Figure 2.14	Same as Fig. 2.12, except for 40-60% centrality.	38
Figure 2.15	Same as Fig. 2.12, except for 60-88% centrality.	39

Figure 2.16	The nuclear modification factor for neutral pions for 0 - 20% most central d -Au collisions at RHIC. The simulation is carried out by binning in centrality according to the number of charged particles produced (prescription B: see text for details). Simulations include shadowing and no energy loss. Experimental data are taken from Ref. [5].	40
Figure 2.17	Same as Fig. 2.16, except for 20-40% centrality.	41
Figure 2.18	Same as Fig. 2.16, except for 40-60% centrality.	42
Figure 2.19	Same as Fig. 2.16, except for 60-88% centrality.	43
Figure 2.20	The fraction of events that shift in or out from each centrality bin as the definition of centrality is changed from binary collisions to number of charged particles produced. The fractional bin shift is plotted as a percentage of the number of events in the original definition with number of binary collisions, as a function of the transverse energy of the detected pion.	44
Figure 2.21	The ratio of the nuclear modification factor of jets produced in d -Au collisions at RHIC. Experimental data are taken from Ref. [6].	45
Figure 2.22	A correlation plot for N_{chg} vs. N_{bin} for dAu events with no hard p_T cut.	46
Figure 2.23	A correlation plot for N_{chg} vs. N_{bin} for dAu events with a hard p_T cut of 50-55 GeV.	46
Figure 2.24	The ratio of the nuclear modification factor of jets produced in p -Pb collisions at the LHC. Experimental data are taken from Ref. [7].	48
Figure 2.25	The ratio of the nuclear modification factor of charged particles produced in p -Pb collisions at the LHC. Experimental data are taken from Ref. [8].	49
Figure 3.1	Code flowchart showing data input/output for each code set	59
Figure 3.2	Plot showing the output spectra of quarks and gluons from PYTHIA for a LHC p - p event, performed using the procedure described in section 3.3.1.	60
Figure 3.3	Plot showing the contributions of each hard p_T bin to the sum of produced charged hadrons in a LHC p - p event.	60
Figure 3.4	An example event produced from the OSU iEBE-VISHNU hydrodynamic simulation (Taken from https://u.osu.edu/vishnu/physics/).	61

Figure 3.5	Leading pion R_{AA} for 200 GeV Au+Au compared to PHENIX data [9] for varying \hat{q}_0	65
Figure 3.6	Leading hadron R_{AA} for 2.76 TeV Pb+Pb 0-5% centrality compared to CMS data [10] with $\hat{q}_0 = 2.4\text{GeV}^2/\text{fm}$	66
Figure 3.7	Jet R_{AA} for 2.76 TeV Pb+Pb 0-5% centrality compared to CMS data [11] with $\hat{q}_0 = 2.4\text{GeV}^2/\text{fm}$	67
Figure 3.8	A plot of the ratio of the in-medium to vacuum production of quarks in gluons in a smooth static medium representative of Au+Au collisions for in-plane vs. out-of-plane results.	68
Figure 3.9	A dN/dp_T histogram plotted for a 100 GeV quark jet in vacuum and in a 4 fm $\hat{q} = 1.0\text{GeV}^2/\text{fm}$ brick for pion production determined by the KKP fragmentation function and the Texas A&M recombination code, as well as for raw quark and gluon production.	69
Figure 3.10	A plot of pion spectra generated using the KKP fragmentation function and the Texas A&M recombination code for vacuum jets and for 0-5% 200 GeV Au+Au collisions.	70
Figure 3.11	Leading pion R_{AA} for 0-5% 200 GeV Au+Au events, generated by using the KKP fragmentation function and by using the Texas A&M recombination code.	70

CHAPTER 1: INTRODUCTION

1.1 The Strong Force and Quantum Chromodynamics

The theory of the strong force is described with Quantum Chromodynamics (QCD). The Lagrangian for QCD that describes the strong interactions is:

$$L_{QCD} = -\frac{1}{4}F_{\mu\nu}^a F^{a\mu\nu} + \sum_q (\bar{\psi}_{qi} i\gamma^\mu [\delta_{ij}\partial_\mu + ig(A_\mu^a t^a)_{ij}] \psi_{qj} - m_q \bar{\psi}_{qi} \psi_{qi}). \quad (1.1)$$

Where the indices μ and ν run from 0 to 3 over the dimensions of space-time, i and j run from 1 to $N_C = 3$ to denote the number of color charges quarks can carry, and a runs from 1 to $N_C^2 - 1 = 8$ denoting the 8 different color configurations for gluons. In this formulation, $F_{\mu\nu}^a$ is the color field strength tensor, ψ is the quark field, g is the coupling of the color field, t^a are the Gell-Mann color matrices, and m_q is the mass of quark flavor q .

The theory itself has a number of parallels to Quantum ElectroDynamics (QED). The mediating gauge bosons of QCD are gluons, much like photons are for QED. Also, similar to how QED has electric charge, QCD has color charge; however there are three of these, called red, green, and blue with corresponding anticharges. These color charges are carried by quarks, just as electrons carry electric charge. A significant difference between QCD and QED is the fact that QCD is a non-abelian theory. Mathematically this means that the description of QCD contains symmetry generators that do not commute (the t^a in the QCD Lagrangian). The QCD Lagrangian is invariant under a gauge transformation of the gluon fields, shown here as:

$$t^a A_\mu^a \rightarrow t^a A'^a_\mu = U(x) t^a A_\mu^a U^{-1}(x) + \frac{1}{g} (\partial^\mu U(x)) U^{-1}(x) \quad (1.2)$$

This has the physical consequence that gluons carry color charge and can couple to each other. This is in contrast to QED where photons are not charged and do not self-interact. A comparison of the Feynman diagrams for the photon vertex in QED and two of the gluon

vertices in QCD is shown in Fig. 1.1 (there is also a 4-gluon interaction that is not shown). The new diagrams lead to a different beta function (which describes the dependence of the coupling on the energy scale of a given process) for the strong coupling constant. This leads to the following formula for the strong coupling constant:

$$\alpha_s(Q^2) = \frac{4\pi}{\beta_0 \ln(Q^2/\Lambda_{QCD}^2)}, \quad (1.3)$$

where Λ_{QCD} is the QCD scale parameter and $\beta_0 = 11 - \frac{2}{3}n_f$. According to the above equation, at lower momentum transfers the coupling continues to grow, until all quarks and gluons are bound within colorless hadrons. On the other hand, processes with high momentum transfer have small coupling and QCD calculations for a portion of these processes can be carried out with perturbation theory.

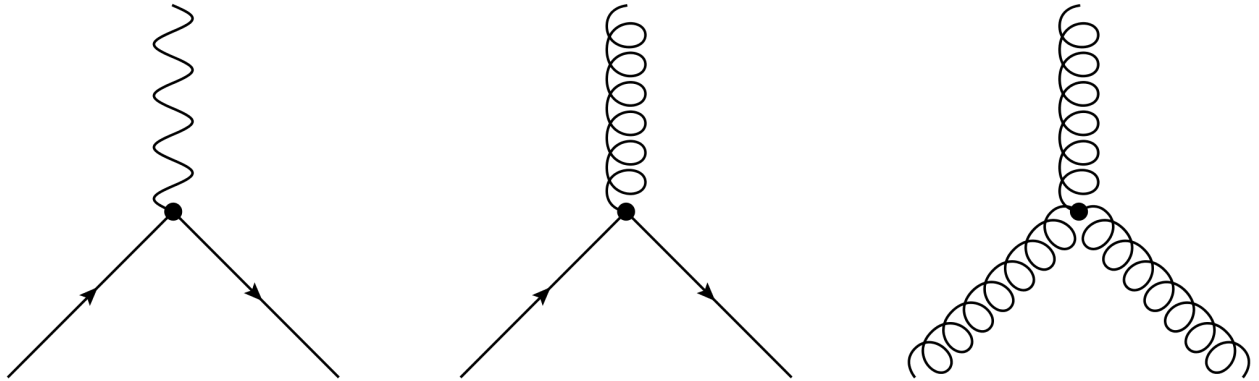


Figure 1.1: Feynman diagrams of QED and QCD vertices; note that while both photons in QED and gluons in QCD couple to charged fermions, gluons can couple to gluons in contrast to photons which cannot couple to other photons.

At low energies, the ever increasing coupling leads to color confinement. This color confinement feature of QCD means that the only particles we can directly detect are bound colorless states. The two simplest color combinations that can produce a net colorless state are a color and its corresponding color anticharge carried by a quark and an antiquark, or a combination of all three colors with each carried by a quark (or three anti-colors carried by three antiquarks). Respectively, the hadrons that are formed in this way are called mesons

and baryons. Attempting to remove a color charge from a net colorless state results in sufficient energy present to materialize at least one quark antiquark pair. This will cause the formation of multiple hadrons, each in a net colorless state. An illustration of this process is shown in Fig. 1.2. With that stated, while a hadron is in a net colorless state it still contains colored objects and is a composite particle. This description implies that there are only two or three quarks present in a given hadron, like the simplistic view of the proton shown in Fig. 1.3a, but there can be more. A hadron can be thought of as being a system of two or three "valence" quarks in a sea of quark antiquark pairs originating from fluctuations, shown in a more realistic illustration of a proton in Fig. 1.3b. One description of the contents of a hadron is in a Parton Distribution Function (PDF) where a parton is just any of the quarks or gluons that can be found in said hadron. The PDF is the number density of partons with a momentum fraction $x = \frac{P_{parton}}{P_{hadron}}$ of the hadron's total momentum at a particular energy scale Q^2 , as shown in Figs. 1.4a and 1.4b.

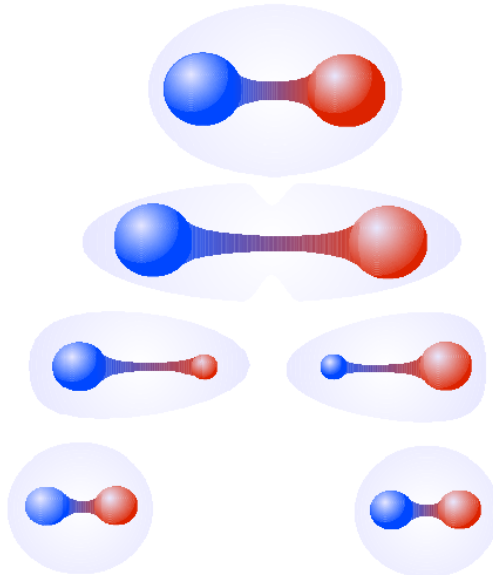
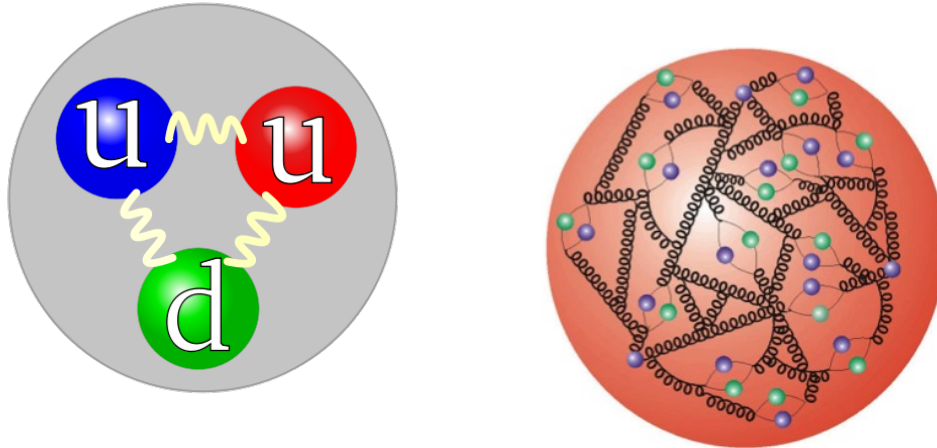


Figure 1.2: An illustration of color confinement: the energy dumped into a system when attempting to remove a colored object from a colorless object results in the creation of a quark-antiquark pair causing the system to collapse into two colorless objects. Taken from <http://webific.ific.uv.es/web/en/content/lattice-qcd-numerical-approach-strong-force>.



(a) The naive view of a proton composed of three quarks bound by gluons. Taken from <https://commons.wikimedia.org/w/index.php?curid=637353>.
 (b) A more accurate view of a proton composed of 3 valence quarks, a number of gluons, and a number of quark-antiquark sea quarks. Taken from http://www.fnal.gov/pub/today/archive/archive_2014/today14-12-18.html.

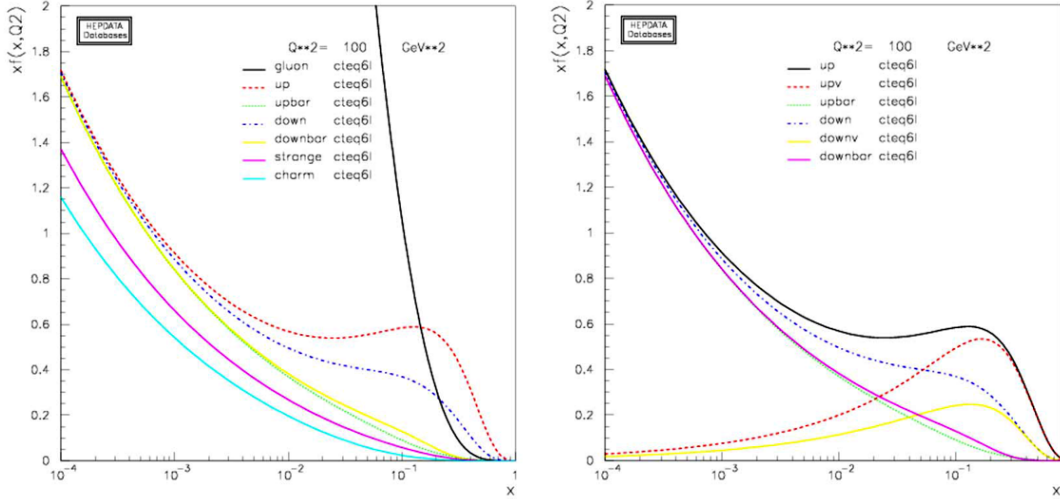
Figure 1.3: Visualizations of the composition of a proton with varying degrees of complexity.

This thesis describes the study of these bound states as well as unbound states of QCD. Bound states are studied in proton-proton ($p-p$) and in proton-nucleus ($p-A$) collisions. To study unbound states of QCD we turn to nucleus-nucleus ($A-A$) collisions.

1.2 Heavy-Ion Collisions and the Quark Gluon Plasma

A form of matter called the Quark Gluon Plasma (QGP) is created in high-energy heavy-ion ($A-A$) collisions. The QGP existed during the early universe and by studying it we can gain insight into the evolution of the universe at just microseconds after the big bang. The QGP is characterized by deconfined color charged quarks and gluons, in analogy to an electromagnetic plasma which contains free electrically charged particles. This is in contrast to normal matter where the quarks and gluons are confined within hadrons, where the net color charge is zero.

The bulk yield of hadrons in heavy-ion collisions both as a function of the transverse momentum p_T and azimuthal angle ϕ can be described using viscous fluid dynamics sim-



(a) A plot of the CTEQ61 [1] parton distribution function for a proton, showing that the proton is composed of not only large x partons (gluons and light quarks) but heavy quarks (charm and strange) as well.[12]

(b) A plot of the CTEQ61 [1] parton distribution function for a proton showing that large x partons tend to be valence quarks and that the total light quark composition has large contributions from the sea quarks, especially at low x .[12]

Figure 1.4: Plots of the CTEQ61 [1] parton distribution function for a proton.

ulations [13][14][15][16]. The yield as a function of azimuthal angle at a given p_T can be decomposed in Fourier harmonics:

$$\frac{d^2N}{dp_T d\phi} = \frac{dN}{dp_T} (1 + 2v_2 \cos(2\phi) + \dots). \quad (1.4)$$

In the equation above, v_2 represents the second Fourier harmonic of this expansion. Calculations of v_2 based on viscous hydro fluid dynamics require a viscosity to entropy density ratio (η/s) close to the theoretical limit of $1/4\pi$, obtained from the AdS/CFT correspondence [17]. This can be seen in Fig. 1.5 where the elliptic flow v_2 was fit for differing values of η/s . The viscosity being inversely proportional to the scattering cross-section, suggests that the QGP acts as a near perfect liquid [2]. The existence of this state lasts for about 10 fm/c or 10^{-23} s in a heavy-ion collision, after which the quarks and gluons hadronize into colorless states and free stream into detectors for measurement.

This is in contrast to p - p and p - A collisions where the densities required for the formation

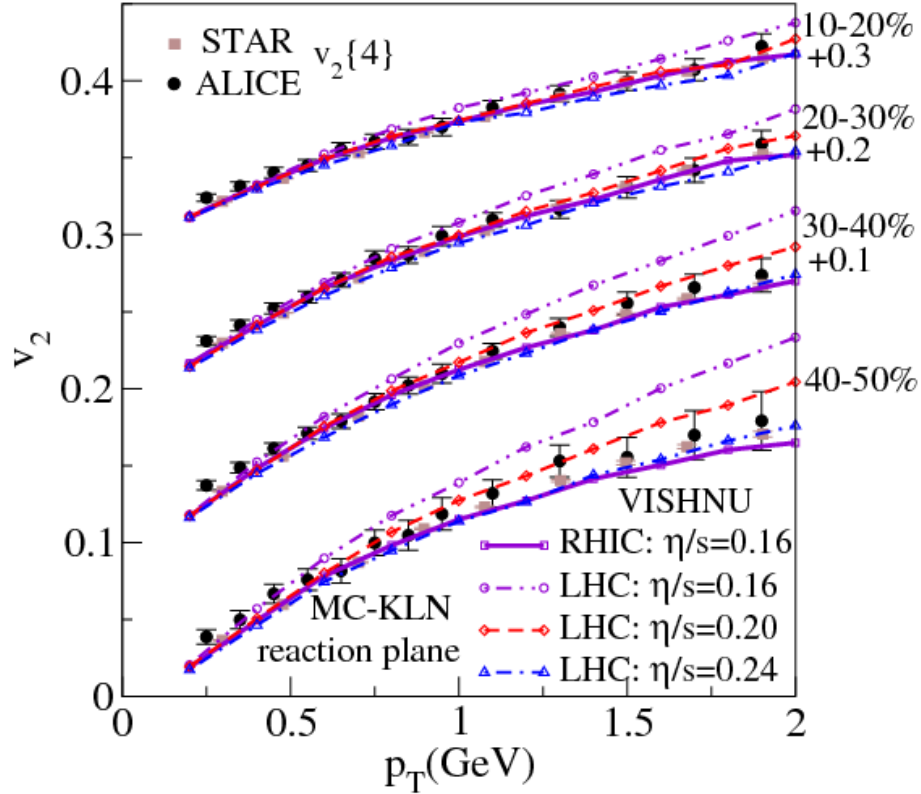


Figure 1.5: A plot of the elliptic flow v_2 at differing centralities for differing values of η/s ; taken from [2]. The experimental data in this plot are from STAR [3] and ALICE [4].

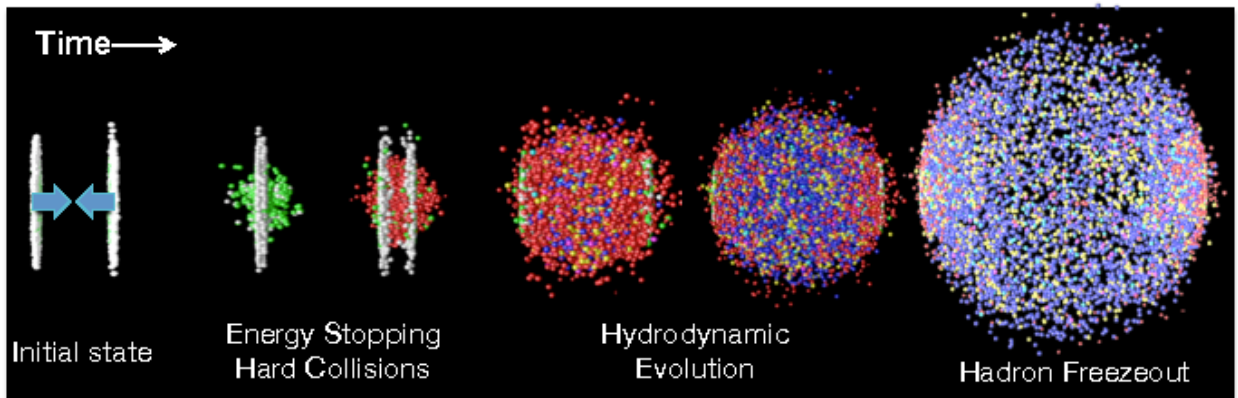


Figure 1.6: An illustration of the different stages of a heavy-ion collision. Taken from <https://arxiv.org/pdf/1201.4264>.

of the QGP are not expected to be reached. A rather straightforward means to classify p - p , p - A , or A - A events, which reveals information regarding the expected density that will be

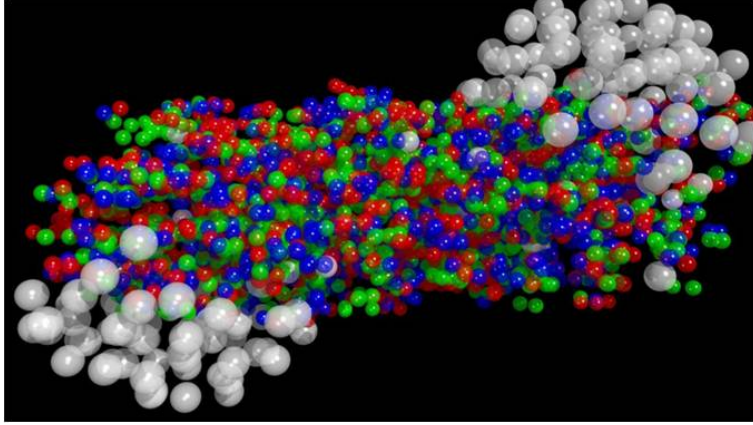


Figure 1.7: An illustration showing non-interacting spectator nucleons escaping the collision and the creation of a colored QGP from the participant nucleons. Taken from http://alicematters.web.cern.ch/?q=town_meeting_062012.

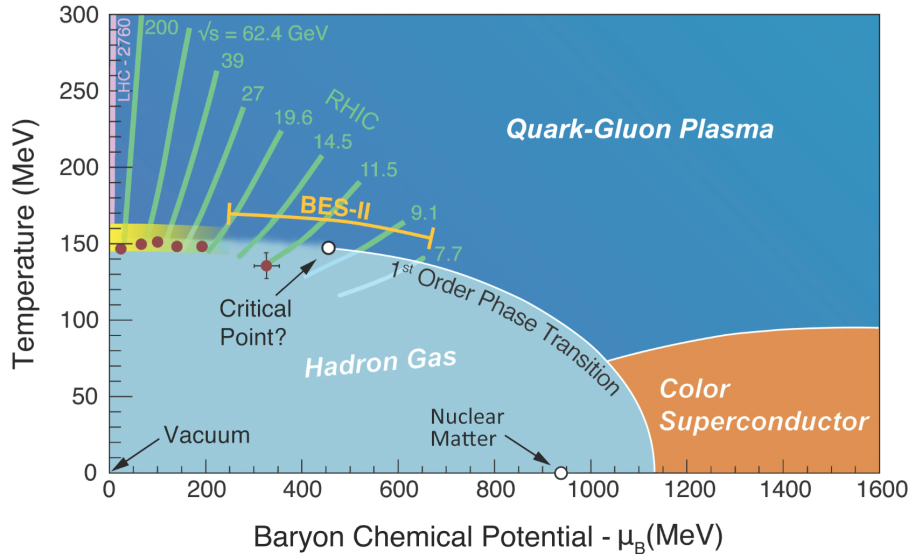


Figure 1.8: A phase diagram for states of matter constrained by QCD. Taken from https://science.energy.gov/~media/np/nsac/pdf/2015LRP/2015_LRPNS_091815.pdf.

produced, is by using the two measures of the number of binary nucleon-nucleon collisions (N_{bin}) in the event and the number of nucleons that participate (N_{part}) in these collisions. In a p - p or p - A event there are only a few (between 1 and 10) collisions and roughly the same number of participants. In an A - A event, both N_{bin} and N_{part} can be on the order of hundreds. This means that there is far more energy in the system during an A - A event

compared to a p - p or p - A event. This higher energy leads to a higher temperature which is required for the formation of the QGP.

The highest densities are expected in central heavy-ion collisions. The centrality is a measure of the impact parameter, where central events are nearly head-on with large numbers of interacting nucleons and peripheral events tend to be glancing collisions with less interactions present. In these systems, while a large number of the incoming partons in the two nuclei simply pass through each other, a considerable fraction are stopped, leading to energy deposited along the path of overlap between the two nuclei. Most of the stopped energy has its origin in the soft gluon fields within each nucleon. As a result the matter produced at mid-rapidity in collisions at RHIC and LHC tend to have almost vanishing net baryon density. The rapidity is a relativistic measure of velocity that is additive under a Lorentz boost and is defined as:

$$y = \frac{1}{2} \ln \left(\frac{E + p_z}{E - p_z} \right). \quad (1.5)$$

The initial deposited energy at mid-rapidity, predominantly composed of gluons, is out of equilibrium at the instant after the two Lorentz-contracted nuclei pass each other. This “medium” equilibrates both kinetically and chemically to form the QGP. The QGP then expands under its thermal pressure, cooling into an equilibrated hadronic plasma, which eventually dilutes sufficiently such that the hadrons decouple from the medium and free stream to the detectors. An illustration of this process is shown in Fig. 1.6 and an illustration of the initial collision with attention paid to spectator nucleons (not in a central collision) is shown in Fig. 1.7 where the Lorentz contraction of the nuclei are ignored.

Almost the entirety of the process described above can be quantified within the framework of relativistic viscous fluid-dynamics [18][19][20][21][22][23]. Estimates of the start time from fitting with experimental data on radial and elliptic flow indicate that the plasma must thermalize within 1 fm/c. This extremely short formation time, is indicative of the extremely

strong interaction in these systems. In current implementations, the equation of state is determined from Lattice QCD simulations [24], and the hadronic phase is simulated using a cascade [25][26]. A phase diagram for states of matter constrained by QCD, including the QGP, is shown in Fig. 1.8.

The QGP thus exists for a very brief period, from about 1 fm/c to approximately 10 fm/c, depending on the size of the system. As a result, studies of the internal structure of the QGP require deep and penetrating probes of the medium. The extremely small viscosity to entropy density, and the very short thermalization time are much shorter than estimates based on perturbative QCD [27][28][29]. This indicates that the medium is strongly interacting, and the degrees of freedom are not quasiparticle quarks and gluons but something else. All estimates of the temperature reached, from both fits to fluid dynamical simulations and the spectrum of photons [30][31] indicates that the temperatures reached in the medium are far higher than the deconfinement transition temperature T_C , as calculated in lattice QCD. As a result, the QCD medium at temperatures from 1 - 3 times T_C has an internal structure that is so far "undetermined".

The leading probes of this medium fall under the category of hard and electromagnetic probes. These include, jets and high p_T hadrons, photons and dileptons, heavy quarks and onia. Each of these is sensitive to different aspects of the plasma. Alternatively, one could say that they sample different correlators of the medium, e.g., photons and dileptons sample the (electric) current-current correlator $\langle J^\mu(x)J^\nu(0) \rangle$, while the suppression of onia in the media is sensitive to the Debye screening length in the medium. Jets and high p_T hadrons are sensitive to the transverse and longitudinal diffusion and drag coefficients. For an on-shell

massless quark or gluon, the transverse broadening transport coefficient \hat{q} is given as:

$$\begin{aligned}\hat{q}(q^-, T) &= \int d^2 k_\perp \frac{k_\perp^2 |\mathcal{M}|^2}{L^-} \\ &= 4\pi\alpha_S \frac{C_R}{N_c^2 - 1} \int \frac{d^2 k_\perp}{(2\pi)^2} \int dy^- d^2 y_\perp e^{-i\frac{k_\perp^2}{2q^-} y^- - i\vec{k}_\perp \cdot \vec{y}_\perp} \\ &\quad \times \sum_n e^{-E_n/T} \langle n | \mathbf{Tr}_{\text{color}} [F^{+\mu}(y^-, \vec{y}_\perp) F_\mu^+(0, 0)] | n \rangle,\end{aligned}\tag{1.6}$$

where C_R is the color Casimir (C_A or C_F) depending on whether the parton is a quark or a gluon. The equation above uses light-cone coordinates and momenta, where $x^\pm = (x^0 \pm x^3)/\sqrt{2}$.

This is the mean squared transverse momentum incurred per unit length that the parton travels through an equilibrated plasma at temperature T with a light cone momentum of $(q^-, 0, 0, 0)$. For a heavy quark with mass M , momentum $(q^-, \frac{M^2}{2q^-}, 0, 0)$ the exponential term changes to $\exp[-iy^-(k_\perp^2 + M^2)/2q^-]$ leading to an altered spatial range y^- for a given light cone momentum. This is indicative of the observation that heavy quarks are sensitive to different transport coefficients than light quarks, such as the elastic energy loss transport coefficient \hat{e} . Of these three penetrating probes, jets and high p_T hadrons (from jets) constitute the leading probes of the QGP today. There is a considerable amount of data available on jets and jet quenching. In contrast to onia suppression, the application of perturbative QCD to jet quenching is now on a rather firm footing. Unlike the case of dileptons and photons there are several unmistakable signatures of the effect of the QGP on the modification of the jet. In the remainder of this thesis jets and jet modification in cold and hot media are discussed.

1.3 Jets and Leading Hadrons

One of the methods available to study quantum scale phenomena is via high-energy scattering; influence the system with a probe and study the output. While the QGP doesn't last long enough to use an external probe, heavy-ion events will occasionally self-generate a

high-energy probe which leads to the production of a jet. The theoretical definition of a jet is a high transverse momentum p_T "hard" parton that fragments into a collimated spray of particles. This is in contrast to the experimental definition where a jet is a specific collection of particles in an event returned by a given jet algorithm. These jets are produced in both heavy-ion collisions and in single proton-proton collisions that do not produce a QGP. This allows for the modification of the jet in the QGP to be compared to a jet in vacuum. An illustration of a dijet event where one of the jets interacts significantly with the QGP is shown in Fig. 1.9.

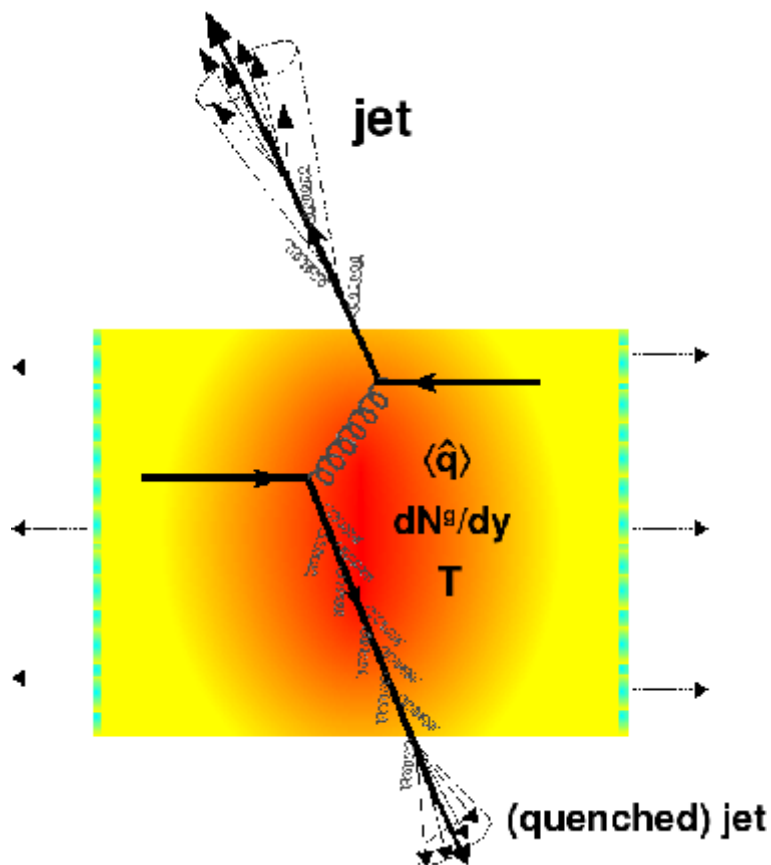


Figure 1.9: A diagram of a dijet event where one jet has significant interaction with the medium. Taken from <https://arxiv.org/pdf/0902.2011>.

In addition, the use of jets allows for the application of perturbative Quantum Chromodynamics (pQCD), since at the energy scale of the jet, the coupling of the strong nuclear force is small enough to use perturbation theory. Jet production involves processes with

small coupling due to the high energies involved as well as processes with large coupling. The analytical calculation of jet observables can be performed by factorization[32][33][34]: nonperturbative effects from the large coupling processes such as the production of the initial high-energy parton (from the parton distribution function) and the formation of hadrons (such as protons, pions, kaons, etc.) are separated from the small coupling processes. The nonperturbative parts can be fit to experimental data and the remaining perturbative parts can be calculated.

One of the observables we have available to measure is the production of high p_T hadrons. The production of these leading hadrons is directly attributable to the presence of the high p_T partons in the jet. This gives one avenue to study the features of a given jet. Since experimental measurement of the production of leading hadrons is more straightforward than full jet production, as no jet algorithm choice is necessary, the associated observables are simpler to directly compare to theoretical calculations.

The cross-section for the production of a hadron h in a general hadronic $A + B$ collision is given by:

$$E \frac{d\sigma}{d^3p}(A + B \rightarrow h + X; s, p_T, \theta_{cm}) = \frac{1}{\pi} \int_{x_a^{min}}^1 dx_a \int_{x_b^{min}}^1 dx_b G_{A \rightarrow a}(x_a, Q^2) G_{B \rightarrow b}(x_b, Q^2) D_c^h(z_c, Q^2) \frac{1}{z_c} \frac{d\hat{\sigma}}{d\hat{t}}(ab \rightarrow cd; \hat{s}, \hat{t}). \quad (1.7)$$

In which $G_{A \rightarrow a}(x_a, Q^2)$ is the parton distribution function that gives the probability of having a parton a with fractional momentum x_a of the hadron A at a momentum scale Q and $D_c^h(z_c, Q^2)$ is the fragmentation function that gives the probability that parton c fragments into a hadron h carrying a fraction z_c of the parton's initial momentum. The limits x_a^{min} and x_b^{min} are found by taking $z_c = 1$ in the constraint $z_c = \frac{x_2}{x_b} + \frac{x_1}{x_a}$ to first find $x_b^{min} = \frac{x_a x_2}{x_a - x_1}$ then taking $x_b = 1$ as well to find $x_a^{min} = \frac{x_1}{1 - x_2}$. For which, $x_1 = \frac{1}{2} \frac{2p_T}{\sqrt{s}} \frac{1}{\tan(\frac{\theta_{cm}}{2})}$ and $x_2 = \frac{1}{2} \frac{2p_T}{\sqrt{s}} \tan(\frac{\theta_{cm}}{2})$.

There is an issue however, that arises during the calculation of this cross section. The

production of leading hadrons is modified by collinear gluon splitting; it suffers from a collinear divergence that must be removed to obtain meaningful results. This is performed by using the fragmentation function to absorb and cancel this divergence, giving it the dependence on Q^2 as seen in equation 1.7.

In the calculation of a full-jet cross-section this issue does not necessarily arise. The presence of a soft gluon should not alter the jet cross-section; it is collinear and IR safe. This results of this calculation need to be compared to experimental results, which depend on the particular jet algorithm used. There are two main types of jet algorithms; these are termed cone and clustering. One of the earliest algorithms used was a cone-type algorithm applied to e^+e^- collisions developed by Sterman and Weinerg [35]. The cross-section for jet production in this formalism is:

$$\sigma(E, \theta, \Omega, \epsilon, \delta) = (d\sigma/d\Omega)_0 \Omega [1 - (g_E^2/3\pi^2)(3\ln\delta + 4 \ln\delta \ln 2\epsilon + \pi^2/3 - \frac{5}{2})]. \quad (1.8)$$

In this equation, ϵ is the small fraction of energy emitted outside of the two back-to-back cones of half-angle δ that form the jets in the event, that are within two fixed cones of solid angle Ω that are at an angle θ with respect to the beamline. The coupling g_E in this formalism is defined at a renormalization point with four-momenta of order E . The cross-section $(d\sigma/d\Omega)_0$ is for the $e^+e^- \rightarrow q\bar{q}$ process in the Born approximation, and can be expressed as:

$$\left(\frac{d\sigma}{d\Omega}\right)_0 = \frac{\alpha^2}{4E^2} (1 + \cos^2\theta) \sum_q Q^2 \quad (1.9)$$

Looking at clustering algorithms, these attempt to combine particles in the event that were likely to be part of the same jet in an event. Of note here are the k_T [36] and anti- k_T [37] algorithms. These work by defining distances between particles (or pseudojets) in the event d_{ij} , and distances for each particle (or pseudojet) relative to the beam d_{iB} . For a given step of the algorithm, these are calculated and the minimum distance measure is found. These

are calculated as:

$$d_{ij} = \min(k_{Ti}^{2p}, k_{Tj}^{2p}) \frac{\Delta_{ij}^2}{R^2}, \quad (1.10)$$

$$d_{iB} = k_{Ti}^{2p}, \quad (1.11)$$

and $\Delta_{ij}^2 = (y_i - y_j)^2 + (\phi_i - \phi_j)^2$. In this formalism, k_{Ti} denotes the transverse momentum of particle i , y_i denotes the rapidity of particle i , and ϕ_i denotes the azimuthal angle of particle i .

If the smallest distance is one of the d_{ij} 's calculated, then elements i and j are combined into a pseudojet. Otherwise if the smallest distance is a d_{iB} then element i is taken to be a reconstituted jet and is removed from the event. This procedure repeats until there are no elements remaining. The main difference in this procedure between the k_T and anti- k_T algorithms is that the distance measures in the k_T algorithm depend on k_T whereas for the anti- k_T algorithm they depend on $1/k_T$. In application, this means that the k_T algorithm starts with soft particles and combines until it reaches the high- p_T particles at the end. This is in contrast to the anti- k_T algorithm which tends to cluster the soft particles only at the end of the process. The effects of this are that the anti- k_T algorithm tends to produce regular consistent geometrically cone-like jets. For the rest of this thesis, the anti- k_T algorithm is used for analysis, unless otherwise stated.

In order to compare analytical approaches of jet modification to experimental data, a Monte-Carlo event generator is extremely useful. This is due to the ability to directly simulate the physical process and to take effective measurements from the simulation, formulated in very close analogy to experimental observables. By simulating events with such a generator, jet observables can be calculated event-by-event and tested against experimental results.

In this work methods to use jet simulations to study both initial and final state effects are outlined. The initial state of a heavy-ion collision was studied by using $d(p)$ - A collisions. These asymmetric collisions are not expected to produce a QGP and so have no final state;

any effects seen are predominately initial state. Final state results were studied with A - A collisions where a QGP is produced.

CHAPTER 2: CENTRALITY DEPENDENT EFFECTS OF JET PRODUCTION IN $d(p)$ - A COLLISIONS

2.1 Introduction

In the context of hard processes in heavy-ion collisions, maximally asymmetric collisions, such as d - Au at RHIC and p - Pb at the LHC, have served the purpose of baseline measurements: Quantifying initial state nuclear effects without the presence of a hot-dense extended final state. Early measurements of suppressed back-to-back hadron correlations, with momenta perpendicular to the colliding nuclei, at the STAR detector at RHIC [38] for Au - Au collisions, compared with a null effect in d - Au (compared with p - p) established jet quenching as a final state effect that takes place primarily in the presence of an extended QGP. These jets with momentum transverse to the incoming beams, were quenched in Au - Au , but were minimally affected in d - Au collisions.

These were consistent with measurements of a lack of suppression in the expected yield of high transverse momentum (leading) hadrons in d - Au collisions at the PHENIX detector [39]. In 2006 the PHENIX collaboration extended this analysis to centrality (the experimental measure of impact parameter) dependent suppression [40, 41]. This data demonstrated an odd enhancement in the yield of high momentum hadrons in peripheral d - Au events. While nuclear effects which modify the dynamics of jet production, were expected in central events, where nucleons from the deuteron encounter several collisions with the large nucleus, these were not expected at all in peripheral events where the deuteron has fewer collisions with the large nucleus.

Recently there have been a series of new measurements, both by PHENIX [41] at RHIC and by ATLAS at the Large Hadron Collider (LHC), on the spectrum of high transverse momentum (high p_T) jets produced in d - Au [42] and p - Pb [43] collisions. The measurements plot the centrality dependent nuclear modification factor R_{dAu} of high p_T jets: A ratio of the detected yield of jets to that expected based on an estimate of the number of nucleon-nucleon collisions in one $p(d)$ - A collision. In both cases, one notices an enhancement in the

R_{dAu} in peripheral events and a "suppression" in central collisions. In a study of the rapidity dependence of the reconstructed jet, by the ATLAS collaboration, it was observed that this peripheral enhancement and central suppression was much more prevalent in the p going direction and vanishing in the Pb direction.

These results are rather counterintuitive. Nuclear effects, in particular those that involve jets and jet production, are expected to be dominant in central events where the initial state engenders several nucleon-nucleon collisions, also the final out going partons have to traverse a more extended medium. Similar arguments may be ascribed to the rapidity dependence of hard particle production, with hard partons traversing longer distances in the nucleus going direction than in the p or d going direction.

An explanation for the observed contradiction to this expectation is that events which lead to the production of a hard jet, requiring an initial state parton with a considerable value of x , have initial states with a fewer number of soft partons, due to the large amount of energy that has been drawn away from the nucleon by the high- x parton. This effect is most pronounced on the partons in the $p(d)$ going direction, and much less on the A going direction as the formation of a hard parton in a single nucleon (in a nucleus) does not affect the soft parton distribution in the remaining nucleons. The higher the x required, the more the suppression in the soft particle production. Thus reactions with very high energy jet production probe the correlation between partons within a nucleon. This sensitivity to multi-parton hard-soft correlations is unique to these experiments, which probe a hitherto unmeasured facet of nucleon structure: Is there a strong correlation between the x values of the leading partons in a given event and the total number of partons in the nucleon in that event. The term "strong" is implying something more than the trivial correlation due to straightforward energy conservation: Is there a kind of *color transparency* in the initial state, for events with a hard jet in the final state? These calculations do not provide a clear answer to this second question. Beyond this, another goal of this work is to provide a reliable parameter free event generator which may be used, with certain caveats, to reproduce at least

some portion of these new data on $p(d)$ - A collisions with jet production. The results of this work will provide detailed input to a more dedicated event generator that will have to be constructed to study such collisions in greater detail.

Continuing, the model is described and how soft particle production is affected by the production of a hard jet is shown. To make direct connection to experiments the PYTHIA event generator [44], which is used extensively to model p - p collisions, was modified. To date there have been several approaches which have attempted to describe this new striking physics result. In Ref. [45], the authors have proposed a similar mechanism of enhancement in peripheral events and suppression in central events but not incorporated it in an event generator framework. In Ref. [46], the authors have proposed that the wave-function of the proton is considerably modified in the presence of a hard parton. In Ref. [47], the authors have attempted to understand the effect of the energy depletion due to jet formation using the HIJING event generator [48, 49]. In none of these calculations, could the authors achieve widespread agreement with the data. This work has been constructed entirely within the PYTHIA event generator, by modifying it. As such, this construction suffers from several constraints which are inbuilt within this particular event generator. The HIJING event generator as in Ref. [47] was not used. The primary reason being due to the resampling of the parton distribution function between collisions; this has the effect of the proton (or nucleon in d - Au collisions) changing its parton distribution function between successive collisions which changes the distribution of soft partons that arise after the hard parton has been extracted.

In the subsequent section we describe the event generator that samples the location of the nucleons in the two incoming nuclei and outline the changes introduced into the PYTHIA event generator. In Sec. 2.3 we present comparisons with experimental data at RHIC and LHC. The conclusions are presented in Sec. 2.4.

2.2 Simulation Details

2.2.1 Sampling the nuclear distribution

Maximally asymmetric collisions such as p - Pb or d - Au represent cases where the experimentally determined centrality of the event appears to be influenced by the production of a hard jet. In order to simulate jet production in such systems, the PYTHIA event generator was modified and extensively used. This modification of the event generator depended on the number of nucleon-nucleon collisions in a given $p(d)$ - A event. This number of collisions was determined using several methods. These methods are described in this section.

Along with a description of this setup, the most naïve explanation of the observed correlation between jet production and centrality is explored and eliminated: That the deuteron due to its large size, often has the proton and neutron far apart and thus cases where a jet is most likely to be produced, when either nucleon strikes the densest part of the oncoming nucleus may coincide with cases where the other nucleon simply escapes without interaction leading to reduced soft particle production. It should be pointed out, in passing, that such a scenario is immediately ruled out by an almost identical correlation between jet production and centrality in LHC collisions, where there is only one proton colliding with the large nucleus.

2.2.1.1 The Deuteron:

Collisions at the LHC always involve a proton colliding with a Pb nucleus. However, at top RHIC energies the collisions are usually that of a deuteron (d) on a Au nucleus. The deuteron is an extremely well studied state in low energy nuclear physics. The wave-function of the deuteron is given by the Hulthén form [50]:

$$\psi_H(r) = \frac{e^{-ar} - e^{-br}}{r}, \quad (2.1)$$

where, $a = 0.228 \text{ fm}^{-1}$, $b = 1.18 \text{ fm}^{-1}$. The probability distribution of a nucleon within

a deuteron is given as,

$$\rho(r) = |\psi_H(r)|^2. \quad (2.2)$$

This distribution is sampled to obtain the positions of the two nucleons.

As is well known, the Hulthén wave-function leads to a rather wide nuclear distribution. This is illustrated in Fig. 2.1, where three representative events are plotted, with both the *Au* nucleus and the deuteron distributions projected on the *z*-axis which is the axis of momentum of the two nuclei. As can be seen from Fig. 2.1. the nucleons in the deuteron may be close together, as well as, a gold radius apart. Due to the large separation between the nucleons, excluded volume corrections were unnecessary but were still included.

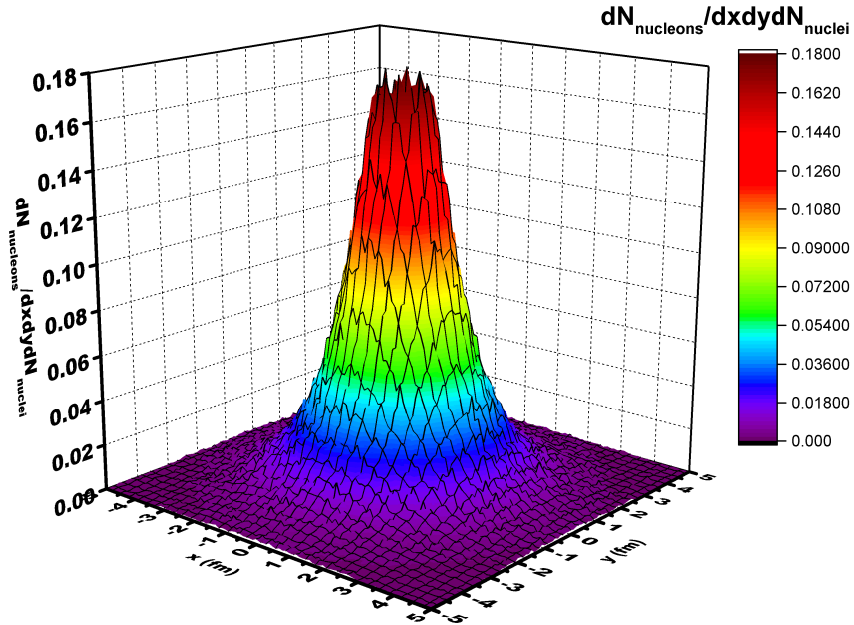


Figure 2.1: The sampled Hulthén distribution for two nucleons in a deuteron.

2.2.1.2 The Large Nucleus (*Au* or *Pb*)

Moving to the nuclear state, there are several methods that may be used to simulate the fluctuating initial state represented by the large nucleus. Only a *Au* or *Pb* nucleus was

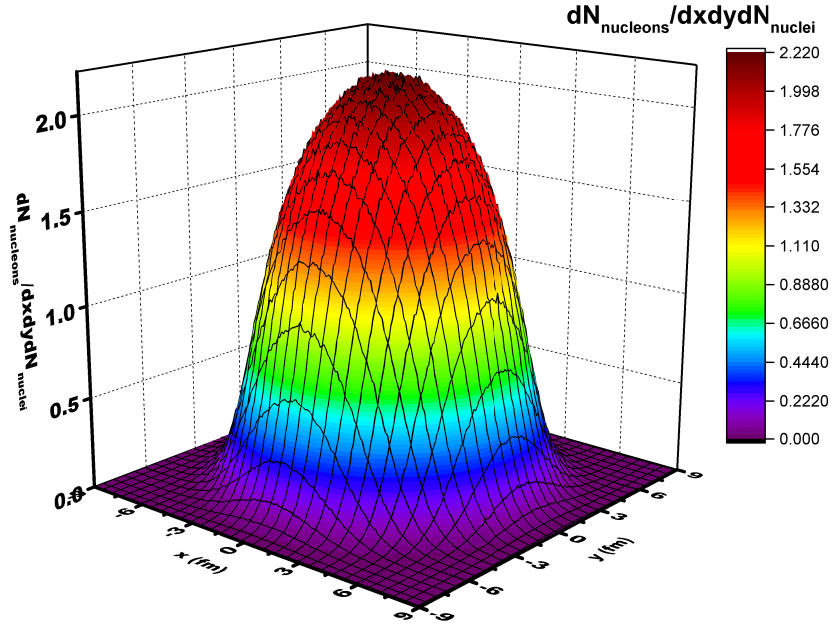


Figure 2.2: The sampled Woods-Saxon distribution for a large nucleus (in this case Au with an $A = 192$.)

considered, as these are studied experimentally. In most cases, the Woods-Saxon density distribution was used, given at a radial distance r as:

$$\rho(r) = \frac{\rho_0}{1 + e^{(r-R)/a}}, \quad (2.3)$$

where ρ_0 is a constant related to the density at the center of the nucleus, R is the radius of the nucleus, and a is the skin depth. These parameters are chosen to match those used by the experiments at RHIC and LHC (for Au , $a = 0.535$ fm, $R = 6.38$ fm; for Pb , $a = 0.546$ fm, $R = 6.62$ fm). The Woods-Saxon distribution of Eq. (2.3) is a single particle distribution. On top of this a nucleon-nucleon correlation is introduced by hand: The excluded volume correction. This is done similar to the method of Ref. [51], where a set of 3 random numbers is generated to isolate the location of a nucleon. If this location is within an exclusion distance of $d = 2R_p$ (twice the proton radius) of another nucleon, then this location is abandoned and another generated. The process is continued until all A nucleons have been included.

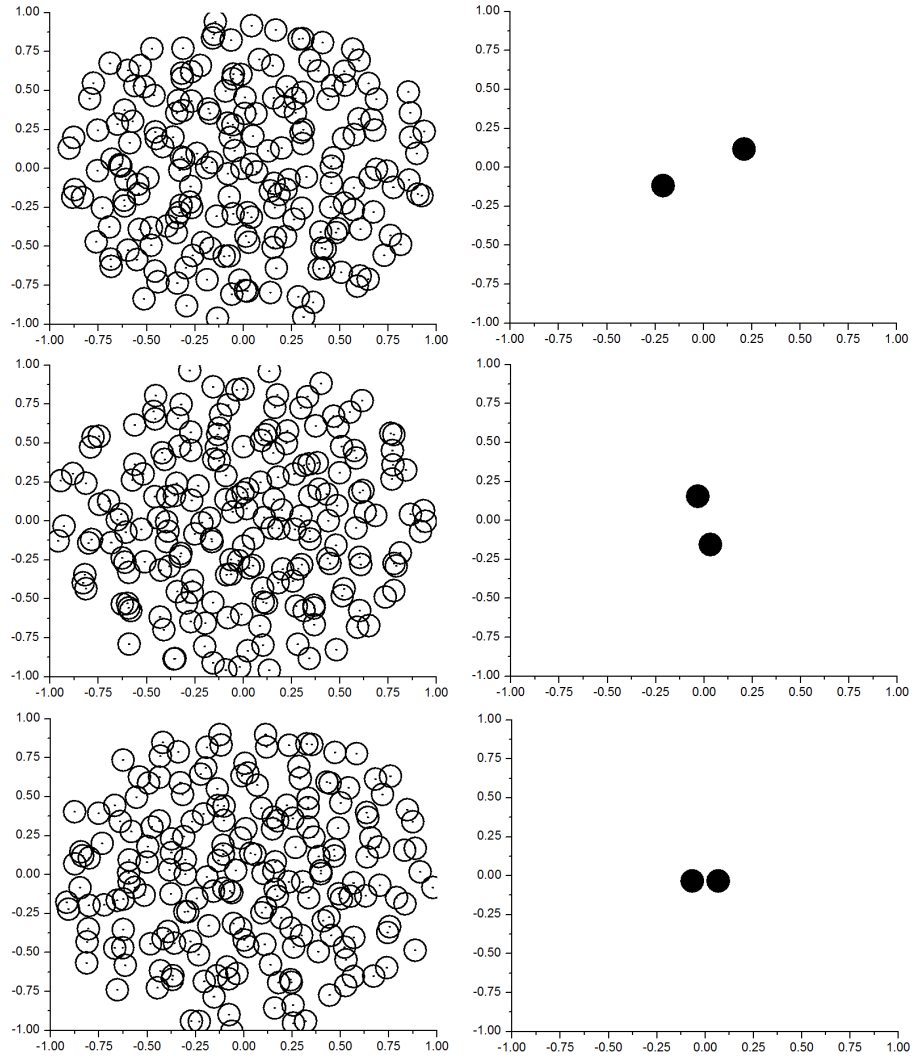


Figure 2.3: Three separate events in d - Au collisions. Nucleon distributions are projected onto the x - y plane.

At the end of this process the center-of-mass of the nucleus is calculated and the nucleus is re-centered.

While only the Hulthén form is used for the deuteron, several probability distributions beyond Woods-Saxon were tried for the nucleon distribution in a large nucleus. These include distributions based on shell-model wave-functions both with and without a modified delta interaction to account for the short range repulsion between nucleons in a nucleus [52] (simple excluded volume). However, none of these enhancements led to any noticeable changes in the final results as compared to the Woods-Saxon distribution with a simple excluded volume. It should be pointed out that for this work solely p - A and d - A collisions have been considered, which only sample the single and two-nucleon distribution within a nucleus. It is entirely possible that the collision of nuclei larger than a deuterium with nuclei smaller than Au may lead to the greater role for multi-particle correlations within a nucleus. There is very little information in nuclear structure on such multi particle correlations. We will not discuss this issue further and only focus on simulations using the Woods-Saxon distribution with an excluded volume.

2.2.1.3 Transverse Size of Nucleons and Binary Collisions:

The nuclear Monte-Carlo generator samples nucleons from the Au (or Pb) side and from the d side and then projects these on the x - y plane as shown in Fig. 2.3. In this work, the transverse size of the nucleons has not been modified with the energy of the collision. The inelastic cross section for nucleon-nucleon scattering is known to grow with collision energy. While centrality selection at the nuclear level is one of the major issues dealt with in this effort, no centrality selection is imposed on the individual nucleon-nucleon encounters. As a result, when a proton from the d overlaps with another from the Au side, no matter how small the overlap, the entire parton distribution function (PDF) of either nucleon is enacted in the collision, i.e., nucleon-nucleon collisions are not expected to have any centrality dependence. In a future effort, an impact parameter in nucleon-nucleon collisions will be used to generate particle production in events where the two nucleons do not overlap completely.

Glancing at Fig. 2.3, it becomes clear that if the transverse size of the nucleons is increased with increasing energy then this will lead to an increase in the number of binary collisions and that will lead to an artificial excess enhancement of the particle production from each individual nucleon-nucleon collision. In this work, the event generator PYTHIA was used to simulate nucleon-nucleon collisions. Within the PYTHIA event generator the cross section increases with energy. To counter the possible artificial increase in particle production with energy, the full cross section generated by PYTHIA is used with no change in the geometric size of the nucleon with the energy of the nuclear collision.

Once both nuclei have been generated, and centers of mass determined, the impact parameter b is simulated with a probability distribution $dP/db^2 = 1/b_{Max}^2$, and the angle of the impact parameter is determined randomly between 0 and 2π . The maximal impact parameter b_{Max} is chosen such that no dependence is observed in minor changes of this quantity. There is no further reorienting of the nuclei. The number of binary collisions can now be determined by simply counting the number of nucleons in the Au side, whose centers are within a transverse distance $d = 2R_p$ of a nucleon in the deuteron. There arise events where not a single collision takes place, these events are dropped from the analysis.

Based on the above considerations, the results of the nuclear Monte-Carlo simulations for a d - Au collisions are shown in Fig. 2.4. In Fig. 2.4, the distribution of events as a function of the number of binary collisions is presented. Following this, events are divided into 4 bins (0-20%, 20-40%, 40-60%, 60-88%) based on the fraction of the total number of events contained in these bins. These bins also correspond to the bins used by the PHENIX experiment. Each of these bins in the number of collisions represents a range of overlapping impact parameters. While this represents the standard method of determining centrality in theoretical calculations or simulations, We will show, in a later section, that this method of determining the centrality of the event leads to results that are not consistent with experimental results for high transverse momentum (high- p_T) pion, charged particle, and jet production at both RHIC and LHC energies.

In this section the focus was mostly on d - Au collisions where both incoming nuclei have to be simulated. In subsequent sections results for p - Pb collisions are shown, where only one nucleus needs to be simulated. There are no other considerations concerning p - Pb that need to be made other than the location of the p is set by the impact parameter b . As pointed out above, no explicit change in the transverse size with energy has been used in this first attempt to understand the behavior of jets in $p(d)$ - A collisions. It should also be mentioned that in all simulations, the isospin of the nucleons has been accounted for.

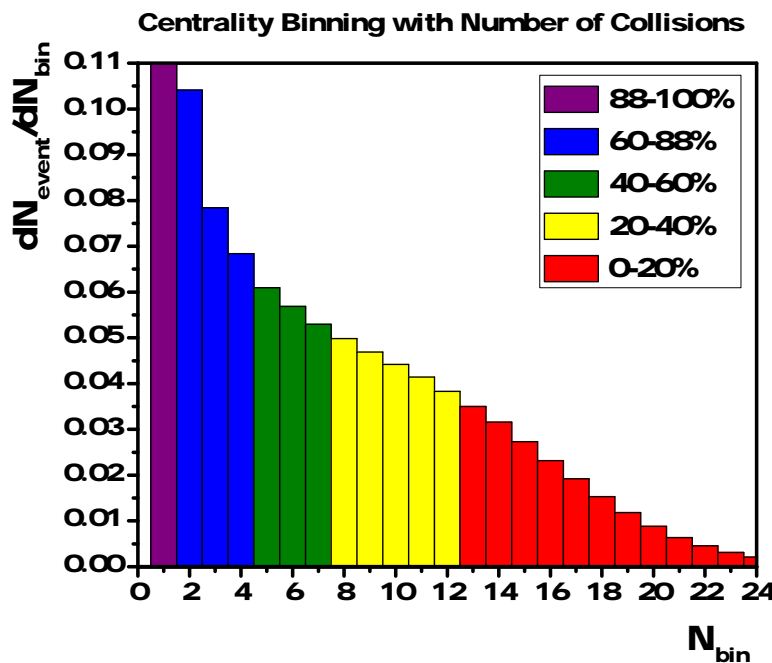


Figure 2.4: The event distribution in d - Au collisions as a function of the number of binary collisions and the division of events in the four different centrality bins.

2.2.2 The Modified Parton Distribution Function

Using the nuclear collision event generator, the number of nucleon-nucleon collisions in each event may be determined. Each nucleon in the deuteron, in a d - Au collision at RHIC, or the proton in p - Pb collisions at the LHC, will potentially engender several collisions with nucleons in the large nucleus. At RHIC the relativistic γ factor is about a 100 while it is close to 2750 at the LHC. At such large boosts, the parton distribution function within the

nucleon is time dilated to distances well beyond the length of the large nucleus. As a result, the parton distribution of the nucleons in deuteron (in a d - Au) collision, or that in the proton in p - Pb collisions is "static" (frozen) as it progresses through the large nucleus. The word static is used to indicate that the parton distribution, though being continuously depleted by collisions with partons in the nucleons from the large nucleus, is itself not undergoing any intrinsic fluctuation in the course of its passage through the large nucleus.

This brings the discussion to the primary point of this section: Consider the case, where, in the course of fluctuations of the PDF, the proton in p - Pb (or one of the nucleons in d - Au) has focused a large amount of energy within a single parton. This parton, in a collision with a similar parton in the oncoming nucleus will produce back to back jets at mid-rapidity. The presence of a parton with such a large energy will lead to less energy being available for the production of other softer partons. As a result, there will be a depletion in the number of soft partons in the proton in p - Pb (or projectile nucleon in d - Au) collisions. A similar situation will occur in one of the nucleons within the large nucleus. As a result, an event with a jet will lead to the production of fewer charged particles.

To simulate this effect, the collision of the p (or any of the nucleons in d) is treated as a string of n nucleons in the large nucleus as a single collision between a nucleon and an object with a larger (modified) PDF. As a result, the PDF of the projectile nucleon is sampled only once. To be clear, there are several methods to carry this out, but for this work only focus on the most expeditious method. In the remainder of this thesis, the collection of n nucleons struck as a single entity by the projectile nucleon will be referred to as a "super"-nucleon.

As a first step to simulate the super-nucleon, the PDF of one of the incoming nucleons is enhanced as $F_S(x) = n_p F_p(x) + n_n F_n(x)$. Where, n_p and n_n are the number of protons and neutrons struck by the projectile nucleon. Along with this the energy of the super-nucleon is also enhanced as $E_S = (n_p + n_n)E$, where E is the energy of the projectile nucleon in the lab frame. This prescription turns out to produce a very faithful description of the soft particle production in d - Au (or p - Pb) collisions. This is illustrated by the increase in the yield of

soft particles with increasing enhancement of the super-proton shown in Fig. 2.5. One notes both an increase in the mean value of charged particle production, as well as an increase in the event-by-event fluctuation in charged particle production, as expected.

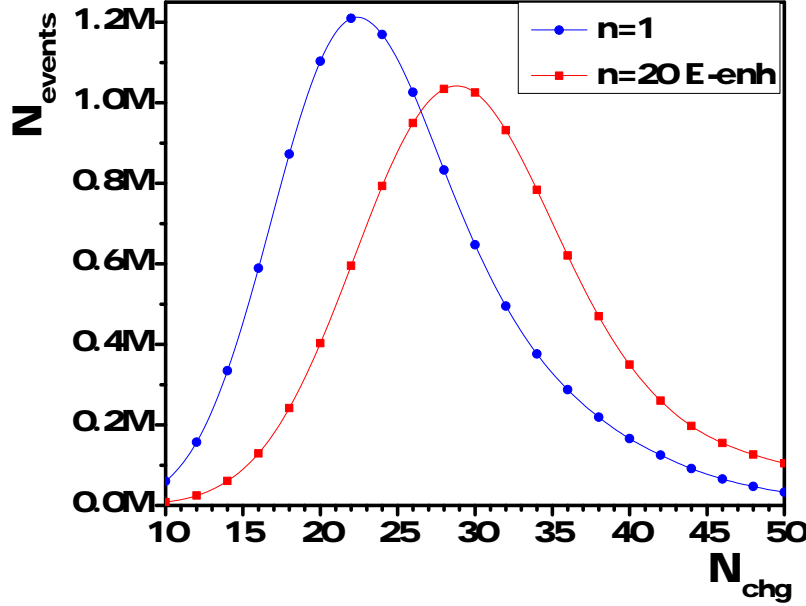


Figure 2.5: The multiplicity of charged particles in a simulated d - Au collision with the Au side simulated as a super-nucleon with a parton distribution function given as $F_S(x) = n_p F_p(x) + n_n F_n(x)$, and energy enhanced as $E_S = (n_p + n_n)E$. In the above plot $n_p = 10$, and $n_n = 10$.

Yet another feature of this formula for the super-nucleon is that it also gives a rather faithful representation of the pseudo-rapidity distribution of the produced charged particles. This distribution for minimum bias events, plotted in Fig. 2.6, shows the "classic" asymmetric double humped structure of the pseudo-rapidity distribution for d - Au collisions at RHIC energies. The overall normalization is less than that measured in actual experiments. However, one should recall that this is generated by modifying PYTHIA where only the interactions between the projectile nucleon and the column of struck nucleons is included. No re-interaction of the produced particles with the remainder of the nucleus is included, and this leads to an obvious depletion in overall particle production. The assumption being

made in comparing these results to experimental data is that even though the overall number of charged particles (or transverse energy) produced is not matched between the simulations and the experiment, the relative distribution between centrality bins will be the same as in the experiment.

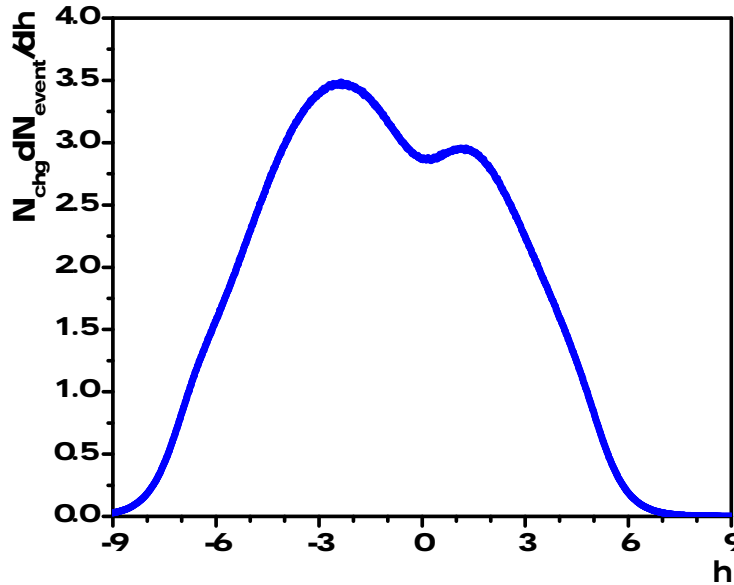


Figure 2.6: The pseudo-rapidity distribution of charged particles in a simulated d - Au collision with the Au side simulated as a super-nucleon with a parton distribution function given as $F_S(x) = n_p F_p(x) + n_n F_n(x)$, and energy enhanced as $E_S = (n_p + n_n)E$.

In spite of the success in soft particle production using the prescription of enhancing both the PDF and the energy of a nucleon in the target nucleus, this procedure leads to an uncontrollable modification to the high momentum (large- x) portion of the PDF (see Fig. 2.7). This is to be expected, as the super-nucleon now has $n = n_p + n_n$ times the energy of a single nucleon, and can thus produce hard partons of higher energy (higher even than the kinematic bound of 100 GeV at RHIC, or 2.75 TeV at the LHC) without the penalty of a rapidly falling PDF. As an illustration of this effect, the ratio of a gluon spectrum from a super-nucleon to that from a regular nucleon was plotted as a function of the ratio of the energy of the gluon to that of the projectile nucleon (un-enhanced nucleon).

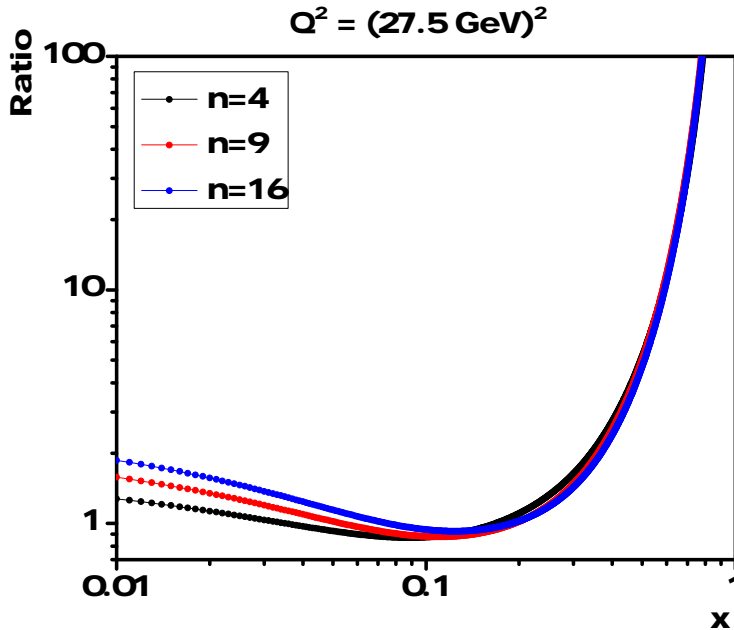


Figure 2.7: The ratio of the gluon distribution in a super-nucleon to that in a nucleon as a function of x , the energy fraction of the gluon, relative to the projectile nucleon.

It is interesting to note that the soft gluon ($x < 0.1$) production is enhanced in the super-nucleon as a function of the total enhancement coefficient $n = n_p + n_n$. There is no enhancement for intermediate energy gluons $x \sim 0.1$, and then an almost n independent enhancement for higher energy gluon with $x > 0.1$. Note that this will of course be broken as one moves past the $x \geq n$, however, since the denominator of the ratio plotted in Fig. 2.7 will vanish, this cannot be plotted in the manner of Fig. 2.7.

Due to this large enhancement in the hard portion of the PDF, this straightforward enhancement of the PDF for a super-nucleon cannot be used. Since the primary focus of these simulations has to do with jet production and its ensuing effect on soft particle production due to energy conservation, We insist on keeping the jet production cross section as close to the reality as possible, and not enhance the energy of the super-nucleon. For comparison with experiment, a more sophisticated enhancement formula for the super-nucleon is used, where the soft portion of the PDF is modified by a shadowing function, and an enhancement

by the number of collisions $n = n_p + n_n$, but no energy enhancement. A shadowing function was also used to modify the super-nucleon PDF event-by-event, depending on the number of nucleons struck by the projectile nucleon. In the case of a d - Au collision, both nucleons may strike multiple nucleons and thus both collisions would be modeled as a nucleon super-nucleon collision. The formula use for this is given as,

$$S(x) = 1 + (R(x) - 1) \frac{N_{coll}}{\langle N_{coll} \rangle}, \quad (2.4)$$

where $N_{coll} \equiv n = n_p + n_n$ is the number of collisions with protons and neutrons encountered by a single projectile nucleon as it passes through the target nucleus in a given event. The mean number of collisions per projectile nucleon is given as $\langle N_{coll} \rangle$. The shadowing factor of $R(x)$ which depends on x and the mass number of the target nucleus A , is taken from Ref. [53]. For the case of a quark it has a rather involved form:

$$R_q^A = 1 + 1.19 \log^{1/6} A (x^3 - 1.2x^2 + 0.21x) \quad (2.5)$$

$$- 0.1(A^{1/3} - 1)^{0.6} (1 - 3.5\sqrt{x}) \exp(-x^2/0.01). \quad (2.6)$$

In Fig. 2.8 the change of the gluon shadowing function is plotted with respect to the number of collisions N_{coll} . As demonstrated in the plot the PDF increases slightly, leading to the enhancement of the number of particles produced in the collision. The plots are normalized with an n dependent constant C_n so that the momentum carried by the gluons in the proton remains the same, i.e.,

$$C_n \int_0^1 dx x R_g^A(x, n) f_g(x) = \int dx x f_g(x). \quad (2.7)$$

This constant is introduced for illustration purposes, to visually demonstrate the enhanced number of partons at $x \gtrsim 0.1$. In PYTHIA simulations (see Ref. [54] for details), a PDF is repeatedly sampled to obtain a series of forward momentum fractions x_i with

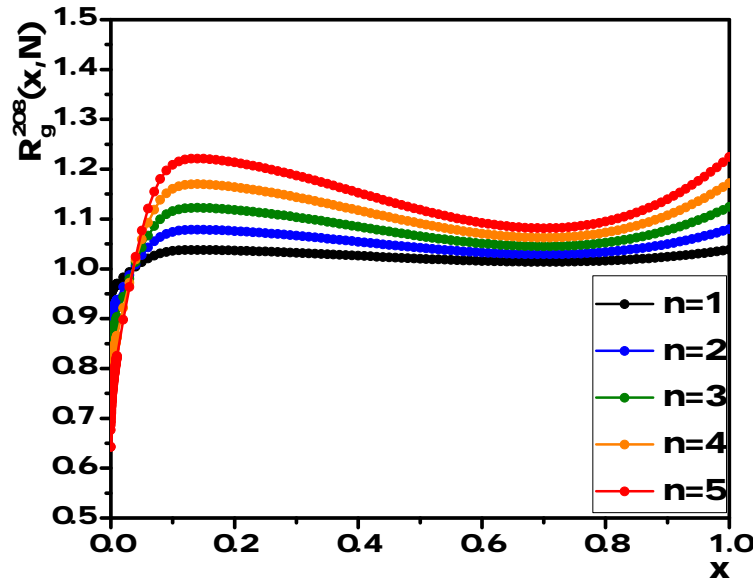


Figure 2.8: The ratio of the shadowed gluon distribution in a super nucleon to that in a regular nucleon as a function of the number of collisions N_{coll} (See Eq. (2.4)). The normalization of each line is adjusted to reflect the function that is sampled by the PYTHIA event generator, which continues to sample distributions until the momentum of the nucleon is exhausted.

$0 < i < N$. Strict energy conservation is enforced by sampling the PDF at the shifted fraction,

$$x'_i = \frac{x_i}{1 - \sum_{j=1}^{i-1} x_j}. \quad (2.8)$$

The process continues until $x'_N \rightarrow 1$, generating N partons. As a result, the numerical sampling is insensitive to any overall constants. However, the number of partons in a given momentum range is sensitive to any changes in the shape of the PDF. As a result, the samplings produce more partons at $x \gtrsim 0.1$.

The PYTHIA event generator has two sources of soft particle production: Beam remnants and hard scattering. In this work, the hard scattering component is modified by introducing an N_{coll} dependent shadowing function [Eq. (2.4)]. This shadowing function enhances the number of hard partons sampled in the $x \gtrsim 0.1$ region. This increases the amount of multi-particle interactions. This leads to more particle production. It should be pointed out that the super-nucleon, in the remainder of this work, has no enhancement in energy and as a result the total energy of the partons sampled in the super nucleon equals the energy of one nucleon.

Without the enhancement in energy of the super-nucleon one does not get the asymmetric distribution of produced charged particles as shown in Fig. 2.6. However, there is still an enhancement in the production of charged particles with increasing number of collisions. While this is somewhat unphysical, the goal of this work is to study the effect of energy conservation on the production of soft particles leading to centrality selection, in conjunction with a hard jet. The production of soft particles is illustrated for p - Pb collisions in Fig. 2.9 where the distribution of the number of charged particles per event is plotted for different number of collisions encountered by the proton. This plot is shown for p - Pb at LHC energies. The effect of the modifications to the super-nucleon PDF has a smaller effect at these energies; the enhancement with increasing N_{coll} is larger at RHIC energies.

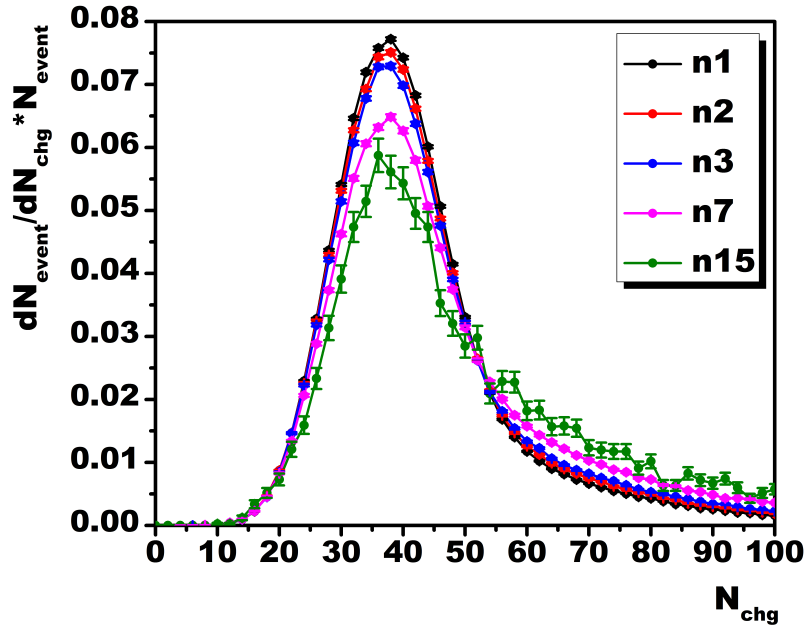


Figure 2.9: The distribution of charged particles produced in a p - Pb collision, as a function of the number of collisions suffered by the projectile proton.

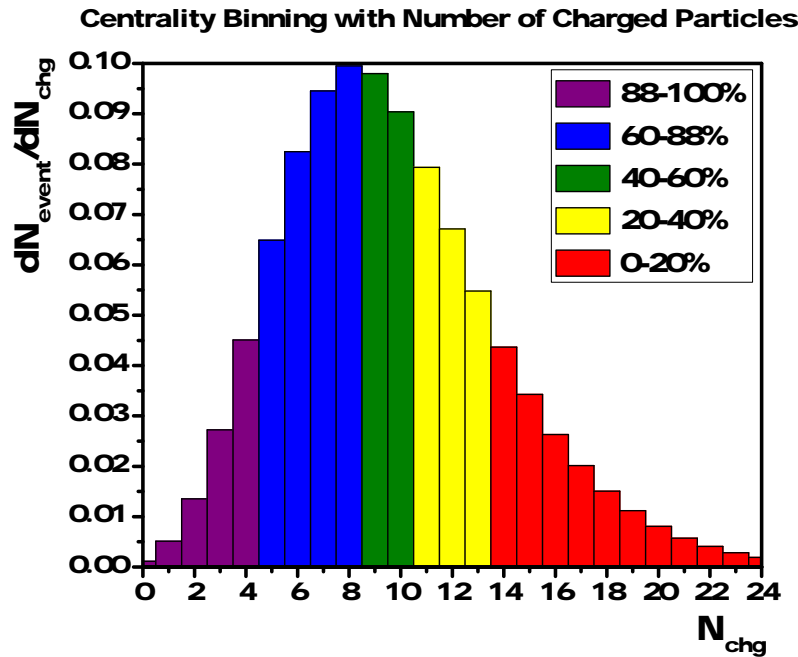


Figure 2.10: The distribution of the number of charged particles produced and the division of the events in the four different centrality bins.

No doubt, this enhancement is proportionately less than that in Fig. 2.5, however, it is sufficient to allow us to bin in centrality. It bears pointing out once again, that in this process of simulating d - Au collisions at RHIC energies, or p - Pb collisions at LHC energies, the soft particle production is in no way commensurate with that in a real d - Au or p - Pb collision. This exercise was performed to demonstrate the effect of a shift in centrality due to the production of a hard jet. We insist on the jet production cross section being unchanged in PYTHIA, while assuming that the reduced soft particle production in this model, as a function of the deduced centrality, is proportional to the particle production in a real collision.

To illustrate this issue, the distribution of the number of events was plotted as a function of the number of produced charged particles in these simulations for d - Au collisions at RHIC energies. As is clearly demonstrated by this figure, there are clear, non-vanishing ranges of particle production, which can be clearly demarcated as centrality bins. These simulations are all done using the *Hard-QCD* switch of PYTHIA. This is the case both for the particle production in general and for particle production in addition to the production of a hard jet. This is done so that the mechanisms that lead to soft particle production both in the presence and absence of a hard jet remain the same in the simulation.

In what follows, jet and leading hadron production at high- p_T is considered and the effects of this on soft particle production are observed. This will be done both for RHIC and LHC energies, for jet production at central rapidities. Charged particle detection, which leads to a centrality determination, will be carried out at all rapidities, i.e., over the entire collision. In actual experiments, charged particles are detected at rapidities far from where the jets are produced, in an effort to remove any correlation between the two processes. Since, in these simulated collisions, the number of particles produced is far fewer than an actual experiment, charged particles at all rapidities are collected, to allow to distinguish between different centralities with higher statistics.

2.3 Results and Experimental Comparison

In the preceding sections, the model used to simulate jet (and high p_T particle) production as a function of centrality in d -Au collisions at RHIC and p -Pb collisions at the LHC, was described in detail. As stated before, the primary goal is two fold: To set up an event generator that may be used to faithfully represent the experimental data on hard soft correlations in asymmetric collisions, albeit with some caveats, as well as to understand the underlying cause of the startling results in such correlations using this new event generator.

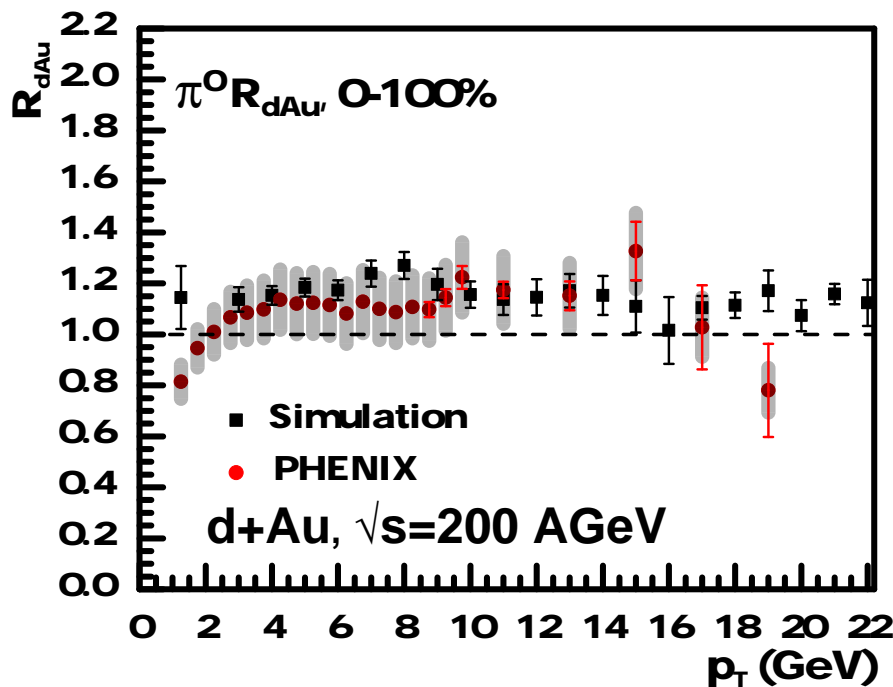


Figure 2.11: The nuclear modification factor for neutral pions for minimum bias d -Au collisions at RHIC. Experimental data are taken from Ref. [5]

Viewed in the lab or center-of-mass frame, it became clear that the nucleon PDF from both the projectile and the target are time dilated, and as such, cannot fluctuate in the short duration of the collision. This necessitated abandoning HIJING [48, 49], and design a new event generator by modifying the PDF of one of the nucleons in a PYTHIA nucleon-nucleon collision. The effects of different modifications within PYTHIA and the overarching nuclear event generator were highlighted in the preceding sections. In the following, the

successes and shortcomings of this new event generator is shown when compared against actual experimental data.

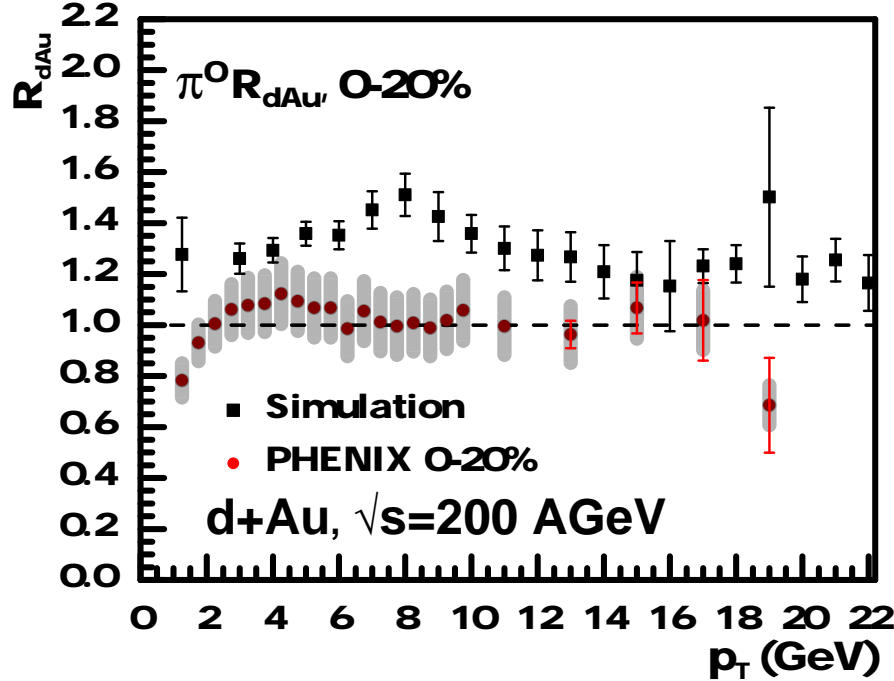


Figure 2.12: The nuclear modification factor for neutral pions for 0 - 20% most central d - Au collisions at RHIC. The simulation is carried out by binning in centrality according to the number of binary collisions (prescription A: see text for details). Simulations include shadowing and no energy loss. Experimental data are taken from Ref. [5]

The first comparisons are carried out for d - Au collisions at RHIC energies. These experimental results were also historically the first to show the odd effect of an enhancement in peripheral events and a mild suppression in central collisions. The data in question are the centrality, p_T and rapidity (or pseudo-rapidity) dependent nuclear modification factor R_{dAu} , defined as,

$$R_{dAu} = \frac{\int_{b_{min}}^{b_{max}} d^2b \frac{d^4 N_{dAu}}{d^2 p_T dy d^2 b}}{\langle N_{bin}(b_{min}, b_{max}) \rangle \frac{d^3 N_{pp}}{d^2 p_T dy}}, \quad (2.9)$$

where N denotes the yield of leading hadrons or jets, binned in transverse momentum, and

rapidity. In the numerator of the above formula, one also integrates over a range of impact parameter b , which in d -Au refers to the 2-D vector from the center of mass of the large nucleus to the center of mass of the deuteron (in Fig. 2.3 for example). The $\langle N_{bin}(b_{min}, b_{max}) \rangle$ in the above formula refers to the mean number of binary nucleon-nucleon collisions per nuclear collision.

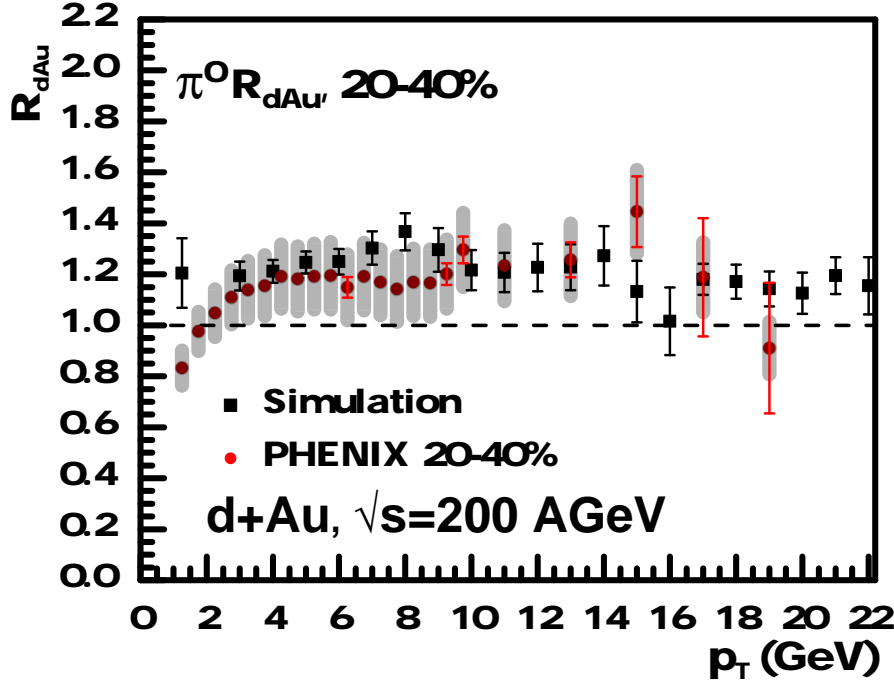


Figure 2.13: Same as Fig. 2.12, except for 20-40% centrality.

As a first step in studying the results of the current simulation in comparison with experimental data, the nuclear modification factor was plotted for minimum bias collisions in Fig. 2.11. Here no division in centrality bins is carried out and thus there is no discussion of determining centrality by number of binary collisions or number of charged particles produced. This serves as a first test of the simulation, which performs extremely well in comparison to the data. The experimental data have been taken from Ref. [5]. Both the simulation and the experimental data show a similar trend: A p_T independent near lack of modification, with the possibility for a minor enhancement between 4 and 16 GeV. This is entirely to be expected, high energy jets are mostly unmodified in cold nuclear matter,

and the minor enhancement can be attributed to the anti-shadowing peak (near $x \simeq 0.1$). It should additionally be stated that in the case of a large centrality dependent modification, as is the case in this model (as well as seen in the experimental data), an unmodified minimum bias R_{dA} is by no means a trivial outcome. This is the first hint that the enhancement in peripheral events is being balanced by the suppression in central events.

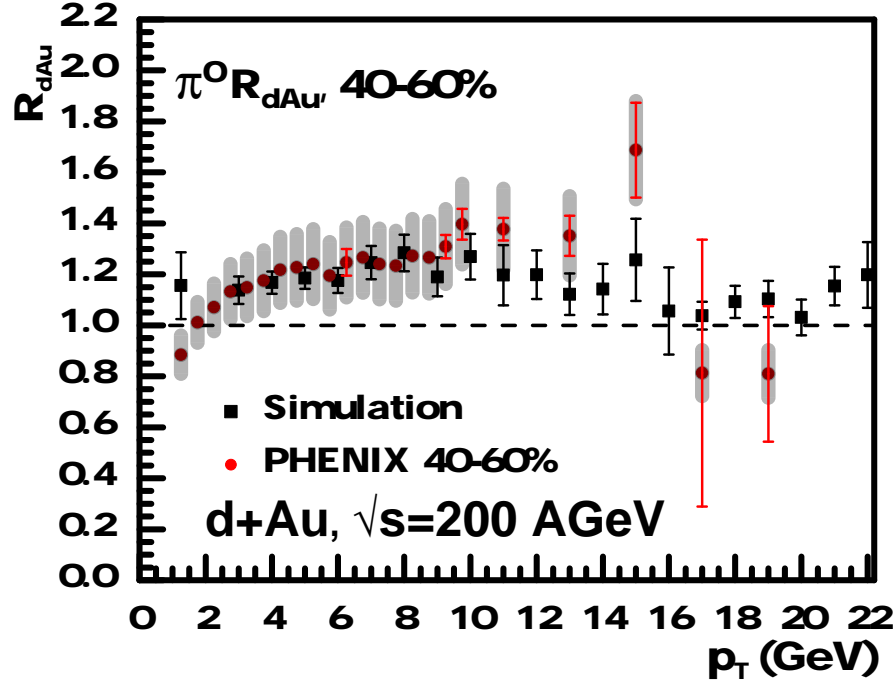


Figure 2.14: Same as Fig. 2.12, except for 40-60% centrality.

The next step is to bin in centrality. This first attempt will follow convention and utilize the number of binary nucleon-nucleon collisions as an indicator of centrality. One runs the nuclear event generator, and collects events, classifying them according to the number of binary collisions. One then bins the event according to where N_{bin} lies in Fig. 2.4. One should point out that while, on average, an increasing $b(\equiv |\vec{b}|)$ leads to a decrease in N_{bin} , any value of b corresponds to a range of binary collisions. This also modifies the numerator

of Eq. (2.9), to

$$\mathcal{N}_A = \sum_{N_{bin}} \frac{d^2 N_{dAu}}{d^2 p_T dy} \theta(N_{bin} - N_{bin}^{min}) \theta(N_{bin}^{max} - N_{bin}), \quad (2.10)$$

where, N_{bin}^{min} and N_{bin}^{max} are set by the centrality bin that we are interested in. The factor of $\langle N_{bin}(b_{min}, b_{max}) \rangle$ is simply replaced by $\langle N_{bin} \rangle$ for the bin in question, and can be calculated from Fig. 2.4. This is referred to as prescription *A* for numerically realizing the numerator of Eq. (2.9).

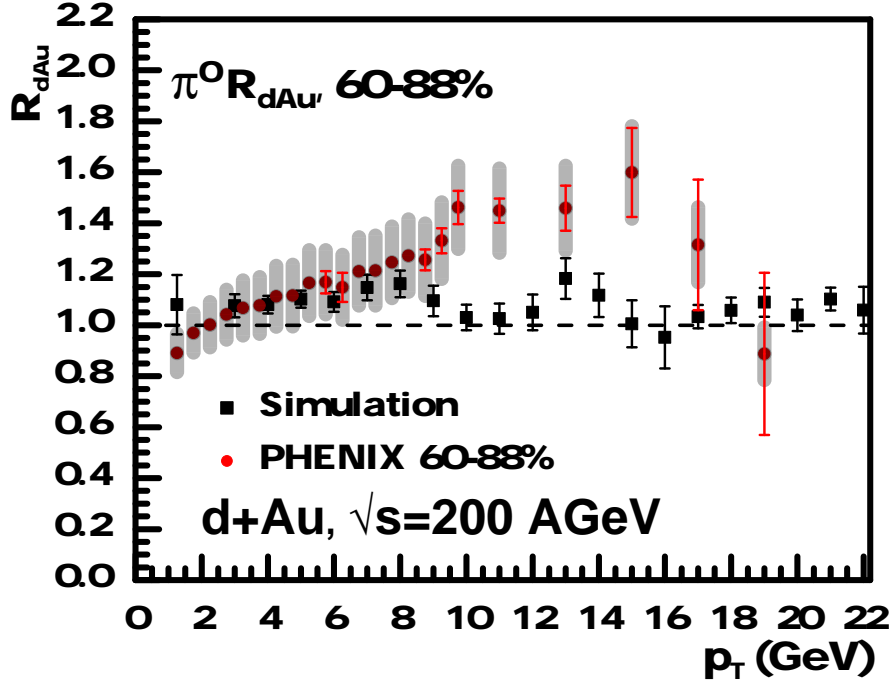


Figure 2.15: Same as Fig. 2.12, except for 60-88% centrality.

An alternate prescription is to classify events according to the number of produced charged particles, utilizing Fig. 2.10 to divide events into different centrality bins. In this case the numerator is replaced with,

$$\mathcal{N}_B = \sum_{N_{ch}} \frac{d^2 N_{dAu}}{d^2 p_T dy} \theta(N_{ch} - N_{ch}^{min}) \theta(N_{ch}^{max} - N_{ch}), \quad (2.11)$$

where, N_{ch}^{min} and N_{ch}^{max} are the minimum and maximum values for charged particles produced, set by the centrality bin that we are interested in. The factor of $\langle N_{bin} \rangle$ in the denominator of Eq. (2.9), now has to be calculated from the collection of events that constitute each centrality bin. This method of calculating the R_{dA} is denoted as prescription *B*.

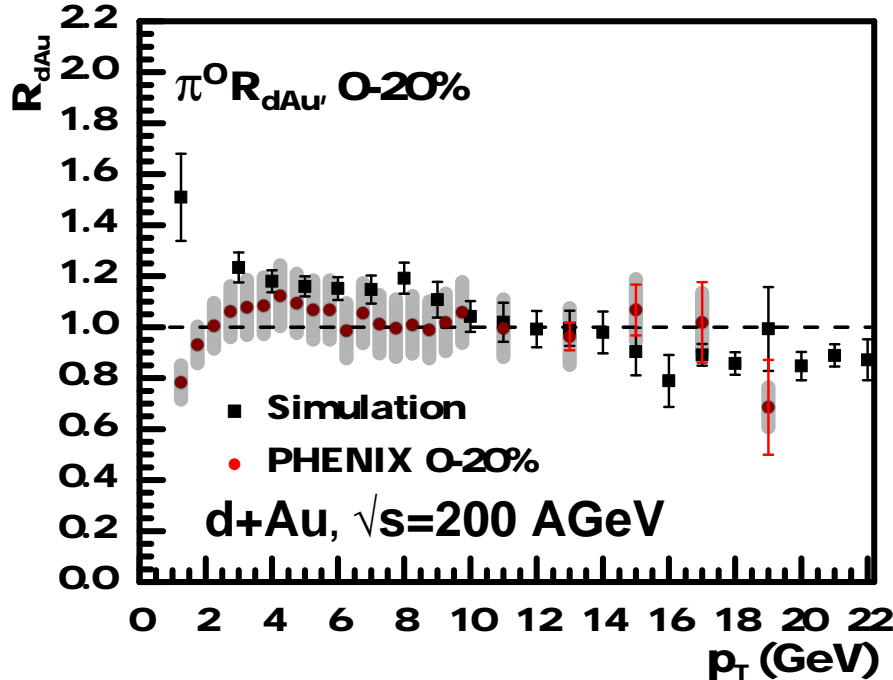


Figure 2.16: The nuclear modification factor for neutral pions for 0 - 20% most central d - Au collisions at RHIC. The simulation is carried out by binning in centrality according to the number of charged particles produced (prescription B: see text for details). Simulations include shadowing and no energy loss. Experimental data are taken from Ref. [5].

Prescription *A* is the usual theoretical method of calculating the centrality dependence of the nuclear modification factor, whereas prescription *B* is closer to the experimental method of determining centrality. Here, the results of simulating the centrality dependence of the pion R_{dA} are first shown using prescription *A* or using the number of binary collisions.

In Fig. 2.12, the R_{dA} for the top 0-20% most central collisions are plotted. One immediately notes an enhancement in the simulation, but no such enhancement in the experimental data, which seem to be consistent with unity. The simulation does not explain the experi-

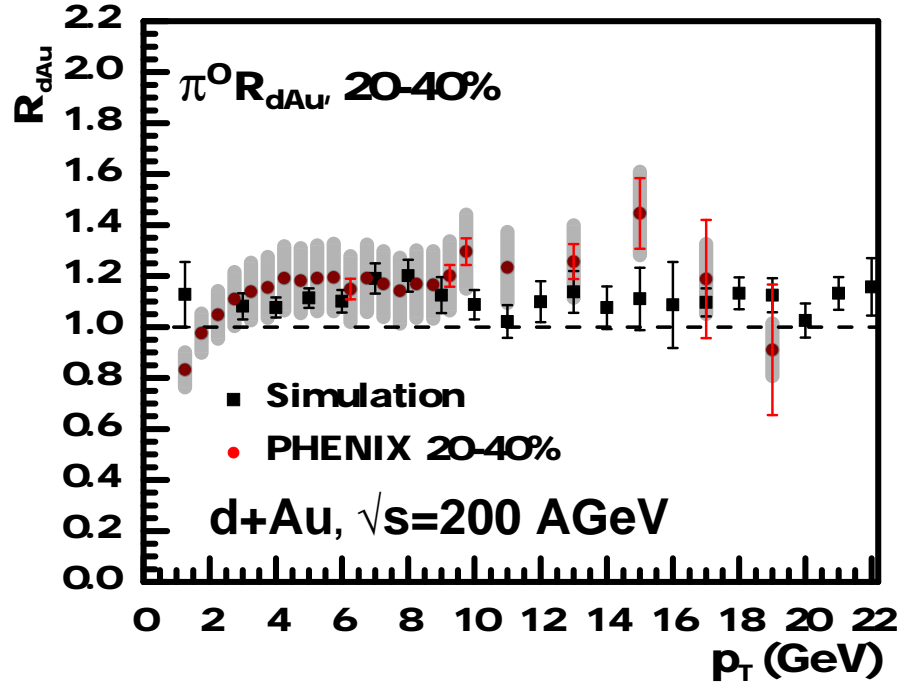


Figure 2.17: Same as Fig. 2.16, except for 20-40% centrality.

mental data. The enhancement in central events such as demonstrated by the simulation, is entirely expected based on the shadowing function that has been used to generate events. Within this framework, the complete lack of any modification in the experimental data is rather surprising; central event should present the maximal nuclear modification.

As one moves up in centrality, from most central to peripheral events, the enhancement seen in the simulation tends to reduce progressively. There is less enhancement in the 20-40% events, even less in the 40-60% simulations, with no modification at all in the 60-88% events, as shown in Figs. 2.13 - 2.15. This behavior of the simulation is entirely expected, moving from cases with the largest expected nuclear density modification to cases with little density and hence no modification at all in the R_{dA} . The experimental data however, show an entirely different trend: With no modification in the central event and the R_{dA} rising with centrality from most central to most peripheral events. The fact that the simulation results with prescription A match some of those from the experiment is entirely coincidental. The simulation for the R_{dA} drops as one transitions from central to peripheral while the data

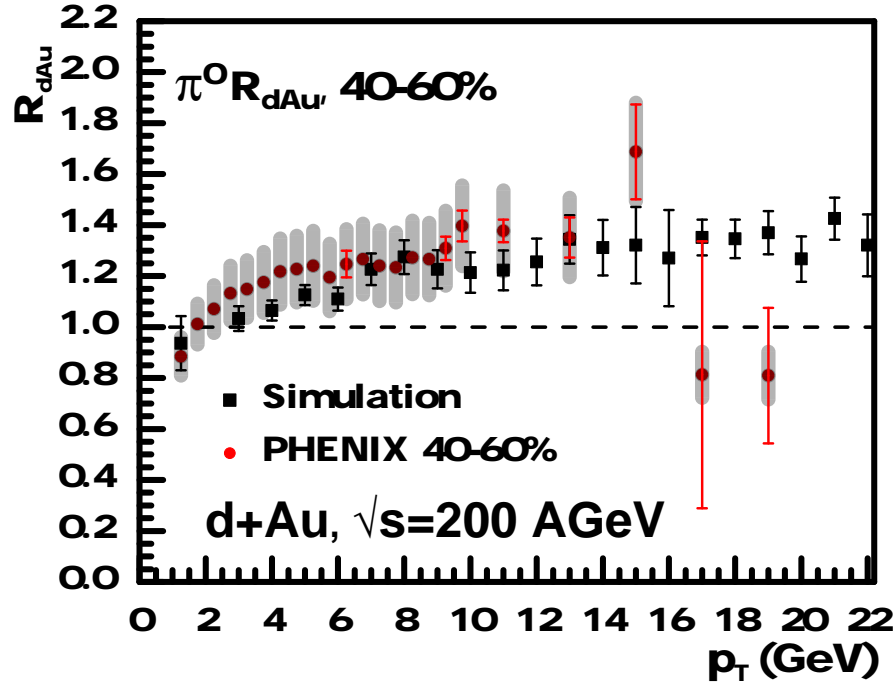


Figure 2.18: Same as Fig. 2.16, except for 40-60% centrality.

trend in the opposite direction.

The experimental results for R_{dA} in d -Au collisions are rather unexpected. The largest modification is seen in the most peripheral bin, which by all accounts should resemble p - p most closely. Continuing, the R_{dA} is calculated using prescription B , i.e., using the simulated number of charged particles produced to bin in centrality. The charged particles are gathered over all rapidities, in events that contain a high- p_T π^0 and then compared with the outlined division in Fig. 2.10. Using this prescription, an excellent agreement is obtained with experimental data on the nuclear modification factor of high p_T neutral pion production. One notes that for central collisions, the R_{dA} is consistent with one and continues to rise as one moves towards more peripheral collisions.

To understand the reason behind the positive comparison between simulation and experiment, We focus on how the events with jets are binned in different centrality bins. In particular, observing how the number of events within each bin change as we transition from binning according to the number of binary collisions to binning according to the number of

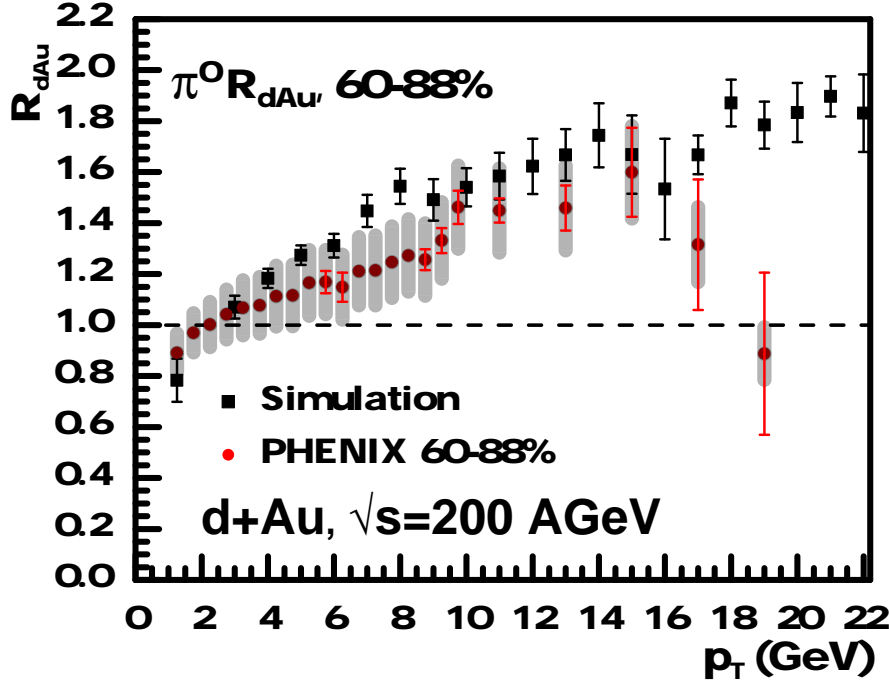


Figure 2.19: Same as Fig. 2.16, except for 60-88% centrality.

charged particles produced. To determine this effect, We focus on events with a high p_T pion and isolate the number of events captured in each centrality bin defined by the number of charged particles produced (prescription B), subtracted from the number of events captured in the same bin defined by the number of binary collisions (prescription A). This difference is then expressed as a fraction of the number of events captured using prescription A . This is plotted as a function of the p_T of the pion in Fig. 2.20. It is seen that central and the number of semi-central (20-40%) events when binned in terms of produced charged particles are suppressed compared to the case when they binned according to the number of binary collisions. These lost events show up in the more peripheral collisions, and lead to an enhancement in those collisions. This is the reason that peripheral events as measured in experiment are enhanced compared to binary scaled $p-p$. Central collisions, compared to binary scaled $p-p$ are slightly enhanced due to shadowing. These lose events to peripheral collisions and as such the yield is reduced, leading to the ratio of central collisions to binary scale $p-p$ to be close to unity.

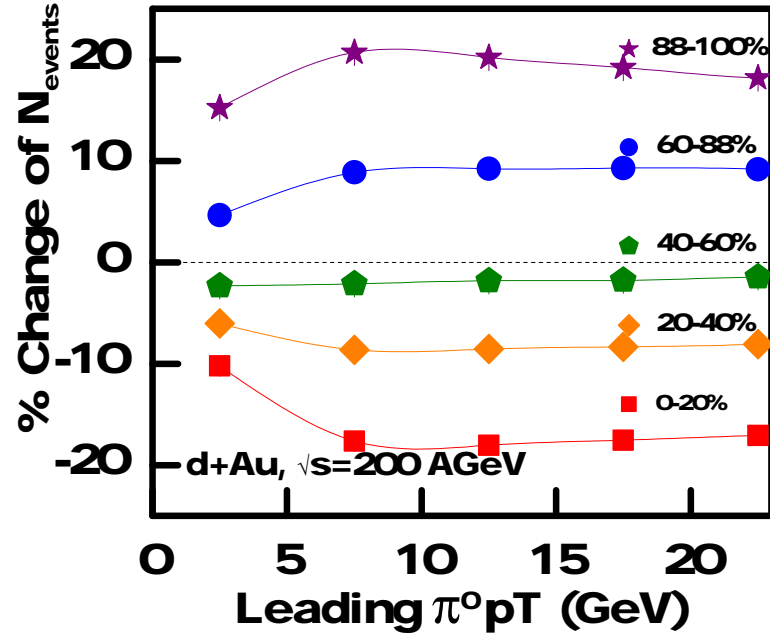


Figure 2.20: The fraction of events that shift in or out from each centrality bin as the definition of centrality is changed from binary collisions to number of charged particles produced. The fractional bin shift is plotted as a percentage of the number of events in the original definition with number of binary collisions, as a function of the transverse energy of the detected pion.

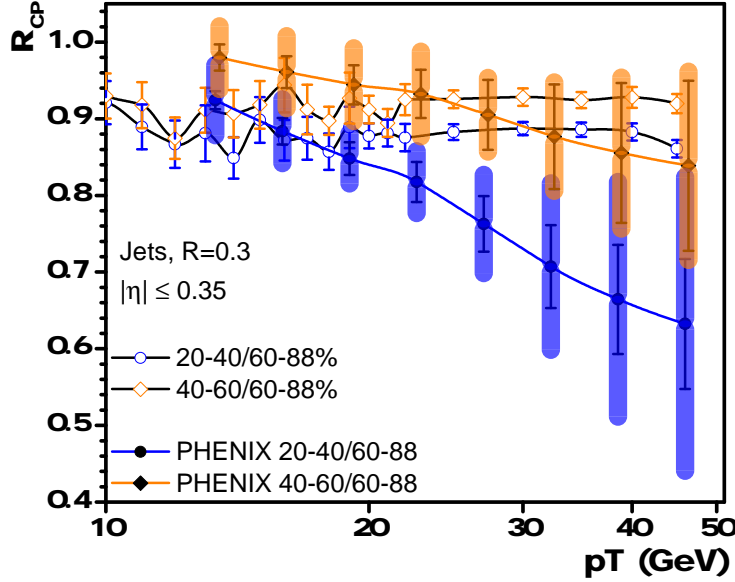


Figure 2.21: The ratio of the nuclear modification factor of jets produced in d - Au collisions at RHIC. Experimental data are taken from Ref. [6].

This “movement” of events from central to less central to peripheral collisions, leads to an enhancement over the expected yield in more peripheral collisions, and a suppression over the expected enhancement in central events. This is mostly an initial state effect. In events with a high p_T π^0 , there has to be a high- x parton in the initial state of at least one nucleon in both the d and the Au nuclei. The presence of a large- x parton in a nucleon of the d depletes the amount of energy available to produce several additional soft partons and as such the collisions of this nucleon with nucleons in the Au leads to the production of fewer charged hadrons. This in turn leads to this event being binned as a more peripheral event.

In addition to further illustrate these effects, a correlation plot of N_{chg} vs. N_{bin} was generated for dAu events with no hard p_T cut and with a rather high hard p_T cut. This was done to show how the distribution of charged particle production changes for a given N_{bin} for events with a jet present. The narrowing of this distribution and shift towards smaller values of N_{chg} should be especially apparent between the two presented plots. This is a

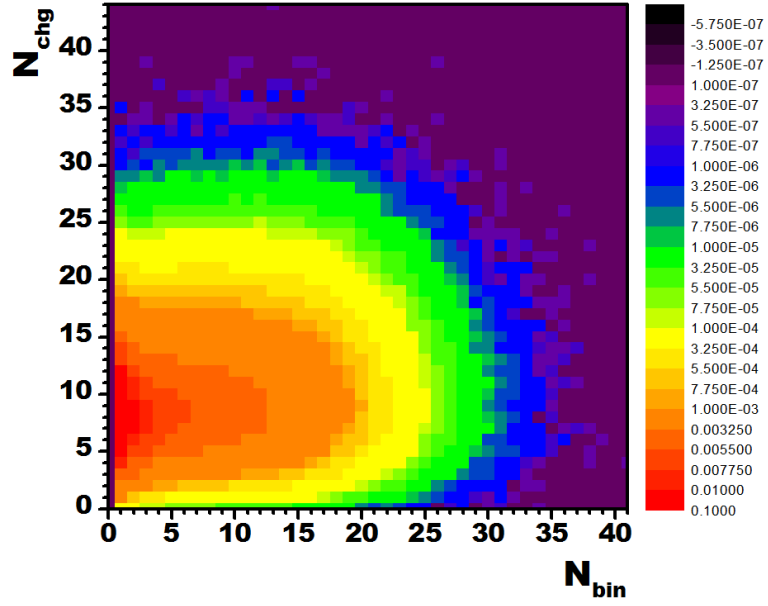


Figure 2.22: A correlation plot for N_{chg} vs. N_{bin} for dAu events with no hard p_T cut.

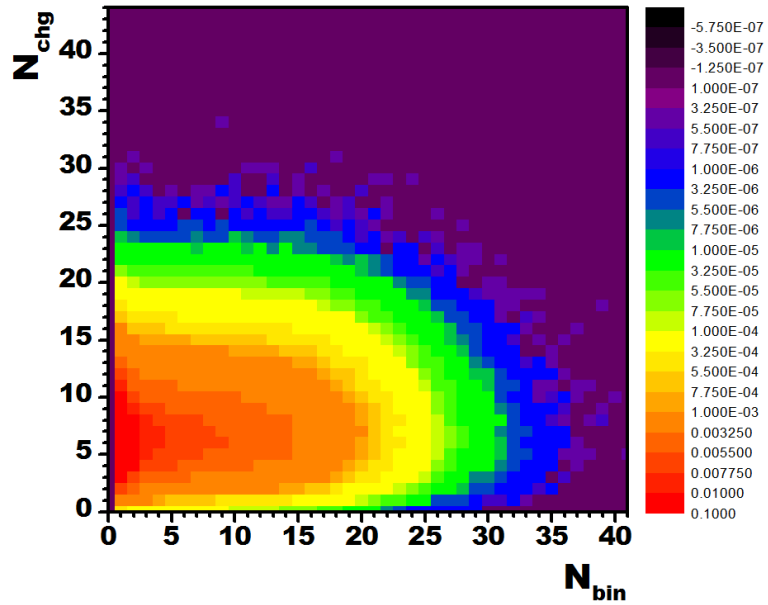


Figure 2.23: A correlation plot for N_{chg} vs. N_{bin} for dAu events with a hard p_T cut of 50-55 GeV.

consequence of the reduced N_{chg} production for events with jet production. These plots are shown in Fig. 2.22 for events with no hard p_T cut, and thus no jets, and in Fig. 2.23 for events with a hard p_T cut of 50-55 GeV.

To test this concept further, the jet R_{CP} , the ratio of the jet spectrum in central to peripheral events, is plotted both scaled by the number of expected binary collisions, as a function of p_T in Fig. 2.21. The results of these simulations are consistent with experimental results if the error bars are accounted for. There is some concern with the 0-20% central data as it does not appear to be consistent between jet and pion measurements, therefore it was omitted from the plot. In addition, the differences in the methods to determine centrality (the experimental results were produced by determining centrality by the charge deposited in the Au-going forward detector whereas this simulation determined centrality by charged particle production over the entire event) as well as in reproducing jets between this simulation and experiment (the jets in the experimental results were reconstructed by applying the anti- k_T algorithm to both electromagnetic clusters and charged particle tracks while rejecting clusters arising from the same particle as a reconstructed track as stated in Ref. [6]) could account for the observed separation. The R_{CP} is suppressed compared to unity as events move out of more central bins towards more peripheral events. This same effect is transferred via fragmentation to the π^0 and manifests in the R_{dA} as discussed earlier.

The primary question at this point is if this effect is solely driven by energy conservation: Is the reduced energy available for the production of small- x partons the only reason for the reduction in the charged particle production, or is there a multi-particle correlation which leads to fluctuation with fewer hard partons, versus fluctuations to several soft partons. In the standard language of pQCD these would be considered as higher-twist multi-parton distribution functions. In an alternative formalism, is this being caused due to an initial state *color transparency* [55, 56, 57]: The fluctuation of the nucleon to a smaller state with fewer hard partons. In order to study this question further, the modification of this process is considered with energy of the collision and with the energy of the jet. The higher the

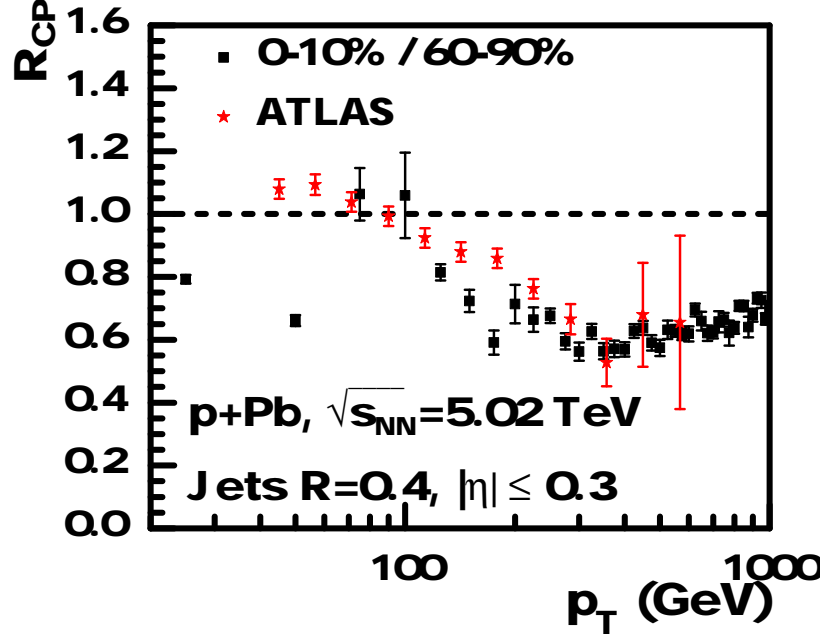


Figure 2.24: The ratio of the nuclear modification factor of jets produced in p - Pb collisions at the LHC. Experimental data are taken from Ref. [7].

energy of the jet, the larger the Q^2 of the process, and as a result, the smaller the size of the fluctuations will be in the proton. This should lead to a more pronounced effect in similar observables at LHC energies with jets or leading hadrons at much higher energies.

In Fig. 2.24, the R_{CP} of jets in central p - Pb collisions is plotted at mid-rapidity, measured by the ATLAS collaboration at the LHC. This represents the ratio of the nuclear modification factor in central events (0-10%) to that in peripheral events (60-90%). At high energies, where the effect of energy conservation should become important, this simulation once again compares very well with the data. In Fig. 2.25, the R_{CP} for charged particles is plotted in a similar range of centrality between central and peripheral collisions. In this case, while the magnitude of the suppression is obtained, the shape of the experimental R_{CP} data is not. Given that on the jet side, the agreement between simulation and experiment starts around 60 GeV, the disagreement between the simulation and data for the R_{CP} of charged particles below a 100 GeV is somewhat puzzling. It should be pointed out that in these cases, there

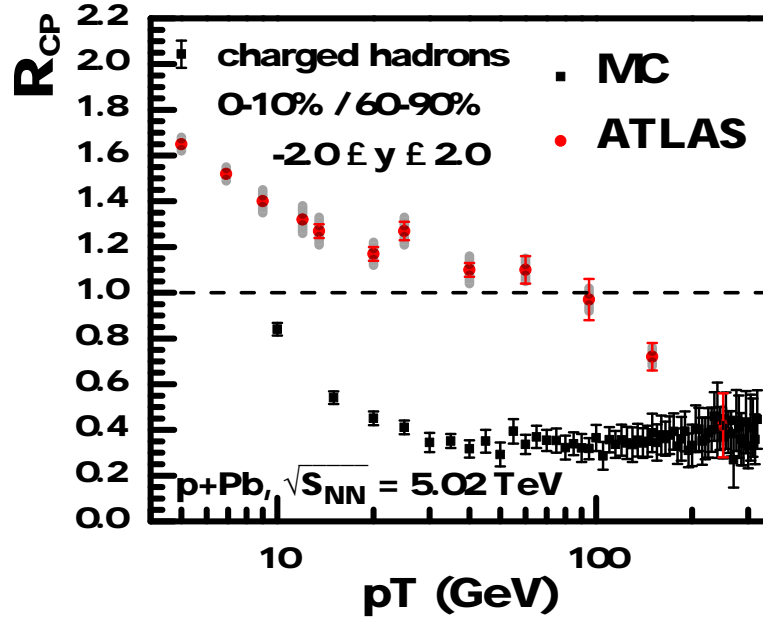


Figure 2.25: The ratio of the nuclear modification factor of charged particles produced in p - Pb collisions at the LHC. Experimental data are taken from Ref. [8].

are a larger number of partons produced, all of which are color correlated. The effect of this on the fragmentation of the leading parton has not been studied in this effort. The effects of color correlation on jet hadronization have been studied in Ref. [58]. As a result, on the basis of these results, whether or not color transparency plays a role in these measurements cannot be stated.

At the risk of repetition, We point out again that our simulations do not in any way contain rescattering and secondary particle production. In the interest of keeping the hard particle production as close to reality as possible (without the need for artificial shadowing), We have abandoned the energy enhanced PDF for the partons in the struck nucleus. There are thus many points of departure between these simulations and the experimental data on soft particle production. The goal in this effort was to point out that events with a hard jet have a lower soft particle production rate, which leads to binning in a more peripheral bin. While this goal is now firmly established, this work should, by no means, be considered

definitive, as these efforts to determine whether color transparency plays a role in these collisions, beyond energy conservation, has not yielded a clear response. These and other topics will be discussed at length in the subsequent section.

2.4 Discussion

In this work, new experimental results from both RHIC and LHC on jet production in extremely asymmetric systems have been discussed. At both the energy scales of RHIC and LHC, similar results were discovered: Events that contained a jet or a high energy particle, seemed to show an enhancement over binary scaled p - p in peripheral events and a suppression compared to the expectation of shadowing and binary scaling enhanced central collisions. The goals in this effort were two fold: The first goal was to set up a reliable event generator that could be used to reproduce some portion of the observed experimental data from such collisions. Based on the success of this event generator, the second goal was to determine if the observed behavior can solely be explained by energy conservation or if it requires the incorporation of correlations similar to that of color transparency.

The designed parameter free event generator consisted of two parts: A nuclear Monte-Carlo to determine the positions of the nucleons within the nucleus, and a modified version of PYTHIA, with an event-by-event shadowing and PDF enhancement to account for the collision of a nucleon from the $p(d)$ with a column of nucleons within the larger nucleus. The results from these simulations, manage to correctly predict the behavior in both the jet R_{CP} and leading particle R_{dA} at RHIC, and the jet R_{CP} at the LHC. The simulation also correctly predicts the magnitude of the suppression in the leading particle R_{CP} at the LHC, though it does not reproduce the shape of the curve. This is a considerable success for such an endeavor. The event generator presented in this effort cannot be considered as complete; there remain several soft observables that, with the given setup of not containing an energy enhanced PDF and without rescattering corrections, cannot be explained. In spite of these, the above study will greatly inform the design of future event generators which will have to be set up to explain these striking experimental data. While this simulation was built on top

of the p - p generator PYTHIA, future generators that incorporate all of the above insights will have to be built as a more original effort.

The goal of setting up the current generator (as well as future generators) was to use it to extract the physics underlying these new observations. These simulations have now established the notion that the enhancement in peripheral events and suppression in central events is entirely due to suppression in soft parton production in a nucleon with a large- x parton. A large portion of this is entirely due to the reduced energy available for soft parton production. Is there any further correlation due to color transparency like effects? The fact that the Q^2 independent shadowing led to a successful description of the jet R_{CP} at the LHC would seem to rule out such an effect. However, the simulation did not manage to explain the shape of the leading particle R_{CP} . Note that both the leading particle R_{dA} and the jet R_{CP} at RHIC energies were mostly accounted for by the simulation. In order to study such a correlation in greater detail, one needs to devise an event generator which will incorporate an energy enhanced PDF, with a far more sophisticated shadowing set up to reproduce the large- x behavior of the PDF within a single nucleon. The set up of such an event generator is left for a future effort. Alternatively, a mechanism will have to be set up where the PDF of the nucleon (or nucleons) from the projectile will have to be sampled once in a $p(d)$ - A collision.

Beyond the study of such initial state color transparency effects, a future more advanced event generator for asymmetric collisions such as d - Au or He^3 - Au will also allow for a deeper understanding of the quantum correlation between nucleons in a nucleus. In this current work, We have explored excluded volume corrections in a Woods-Saxon distribution, as well as Gaussian perturbations in a shell model based distribution. Experimental data, coupled with theory uncertainties at the partonic level do not allow to distinguish between the different correlations between nucleons. However, these can be studied systematically, once the partonic component is settled via p - A collisions. This will allow an extension of nuclear structure which has so far not been extensively studied.

Extremely asymmetric nuclear collisions with a hard interaction provide a new window into a large variety of correlation phenomena at multiple scales. Future studies with more accurate experimental data, as well as a more sophisticated event generator, will reveal new information regarding the correlation between partons within a single nucleon, as well as correlations between nucleons in large nuclei. The current work represents a bench mark in this direction, providing a glimpse of the insights that may be gained by such a research program as well as highlighting the ingredients and framework required for future efforts.

CHAPTER 3: EVENT-BY-EVENT SIMULATIONS OF JET MODIFICATION IN A - A COLLISIONS

3.1 Introduction

This chapter details the study of full A - A events and the effects of the Quark Gluon Plasma (QGP) on jet production; the study of final-state nuclear effects. The ultimate goal of studying heavy-ion collisions is to examine the properties of the QGP. As stated in the introduction chapter, the QGP is a form of matter characterized by deconfined quarks and gluons that appear in these collisions. One of the methods available to study the QGP is by determining the modification of jets due to the presence of this medium. A jet, for the purpose of this section, is a collection of particles defined by some type of jet algorithm originating from a high transverse momentum (p_T) parton.

In order to compare analytical approaches of jet modification to experimental data, a Monte-Carlo event generator is extremely useful due to the ability to directly simulate the physical process and to make "measurements" from the simulation, formulated in very close analogy to experimental observables. There are several other preexisting simulations; Q-PYTHIA [59] which is based on the Armesto-Salgado-Wiedemann (ASW) scheme [60][61][62][63][64] and MARTINI [65] which is based on the Arnold-Moore-Yaffe (AMY) scheme [66][67][68][31][69][70] in addition to formalisms used to directly calculate observables such as the Gyulassy-Levai-Vitev (GLV) scheme [71][72][73][74][75][76]. There are also a number of event generators that are not strictly based on analytical models, including JEWEL [77][78], YaJEM [79][80], and PYQUEN [81] which include medium effects by manually modifying various matrix elements. Generally, these simulations have handled the inclusion of a medium by taking a vacuum event generator and to either add the modification of the jet due to the medium on top of a full vacuum shower, or to alter the vacuum shower generation in such a way that both vacuum radiation and medium induced radiation are performed concurrently.

However, in addition to the technical construction of including a medium, there are two

issues that should be considered when adding medium effects to a simulation. The first of which is constructing the space-time structure of the shower since the medium itself has a space-time structure. The second is a modification of hadronization; the shower partons can potentially recombine with partons from the thermal medium. These two issues are not addressed in a copacetic fashion in the schemes mentioned previously, though it should be noted that YaJEM has phenomenologically incorporated fluctuations in space-time structure [82].

The event generator presented here is based on the Higher-Twist scheme [83][84][85][86][87]. There is also attempt here to include a consistent space-time structure with fluctuations within the simulation. The Higher-Twist scheme itself is applicable to high energy, high virtuality partons, in contrast to the other schemes (AMY and ASW) that are more applicable to lower virtuality (though still high energy) partons. This simulation is constructed with PYTHIA [44] to sample the initial high p_T parton, the OSU (Ohio State University) hydrodynamic simulation iEBE-VISHNU [19] to provide the thermal medium, and the MATTER event generator [88] for jet quenching. In the remainder of this chapter, We will briefly discuss the Higher-Twist model, discuss details of this event generator, and present some preliminary results from the simulation compared to experimental data.

3.2 Theory of Jet Energy Loss

A brief discussion of the theoretical framework used in this event generator begins with the work performed by Guo and Wang [89][90]. For the deep inelastic scattering (DIS) process

$$e(L_1) + A(p) \rightarrow e(L_2) + h(l_h) + X \quad , \quad (3.1)$$

L_1 is the four momentum of the incoming electron, L_2 is the same for the outgoing electron, p is the momentum of a nucleon in nucleus A , and l_h is the momentum of the outgoing hadron. Working in the infinite momentum frame, the momentum of the virtual photon and

the nucleon are:

$$q = [-Q^2/2q^-, q^-, 0, 0] \quad (3.2)$$

$$p = [p^+, 0, 0, 0] \quad . \quad (3.3)$$

The virtual photon γ^* has momentum $q = L_2 - L_1$ and $z_h = \frac{l_h^-}{l_q^-}$ is the momentum fraction carried by a produced hadron. Also, the Bjorken variable x_B is taken as $x_B = Q^2/2p^+q^-$.

The cross section for this process can be stated as:

$$E_{L_2} E_{l_h} \frac{d\sigma_{DIS}^h}{d^3L_2 d^3l_h} = \frac{\alpha_{em}^2}{2\pi s} \frac{1}{Q^4} L_{\mu\nu} E_{l_h} \frac{dW^{\mu\nu}}{d^3l_h} \quad , \quad (3.4)$$

where $s = (p + L_1)^2$ is the invariant mass of the system. $L_{\mu\nu}$ is the leptonic tensor and it is:

$$L_{\mu\nu} = \frac{1}{2} Tr[\gamma \cdot L_1 \gamma_\mu \gamma \cdot L_2 \gamma_\nu] \quad . \quad (3.5)$$

For DIS, the leading twist contributions at lowest order come from a single hard $\gamma^* + q$ scattering. In this case, the semi-inclusive hadronic tensor $\frac{dW^{\mu\nu}}{dz_h}$ at leading twist can be expressed as [91]:

$$\frac{dW_{\mu\nu}^{S(0)}}{dz_h} = \sum_q \int dx f_q^A(x) H_{\mu\nu}^{(0)}(x, p, q) D_{q \rightarrow h}(z_h) \quad . \quad (3.6)$$

In this equation, $f_q^A(x)$ is the quark distribution function:

$$f_q^A(x) = \int \frac{dy^-}{2\pi} e^{ixp^+y^-} \frac{1}{2} \langle A | \bar{\psi}_q(0) \gamma^+ \psi_q(y^-) | A \rangle \quad . \quad (3.7)$$

Also, the quark fragmentation function $D_{q \rightarrow h}(z_h)$ is:

$$D_{q \rightarrow h}(z_h) = \frac{z_h^3}{4l_h^-} Tr[\gamma^- \hat{d}_{q \rightarrow h}(z_h, l_h)] \quad . \quad (3.8)$$

Which, in this equation, $\hat{d}_{q \rightarrow h}(z_h, l_h)$ is:

$$\hat{d}_{q \rightarrow h}^{\alpha\beta}(z_h, l_h) = \sum_S \frac{l_h^-}{z_h^2} \int \frac{dy^+}{2\pi} e^{-il_h^- y^+ / z_h} \langle 0 | \psi_q^\beta(0) | h, S \rangle \langle h, S | \bar{\psi}_q^\alpha(y^+) | 0 \rangle . \quad (3.9)$$

The hard part of the $\gamma^* + q$ partonic scattering is:

$$H_{\mu\nu}^{(0)} = 4\pi e_q^2 [x_B e_{\mu\nu}^L - \frac{1}{2} e_{\mu\nu}^T] \delta(x - x_B) \quad (3.10)$$

where the transverse tensor is defined as

$$e_{\mu\nu}^T = g_{\mu\nu} - \frac{q_\mu q_\nu}{q^2} , \quad (3.11)$$

and the longitudinal tensor is defined as

$$e_{\mu\nu}^L = \frac{1}{p \cdot q} [p_\mu - \frac{p \cdot q}{q^2} q_\mu] [p_\nu - \frac{p \cdot q}{q^2} q_\nu] . \quad (3.12)$$

For higher twist calculations, the hadronic tensor can be expressed as

$$\begin{aligned} \frac{dW^{\mu\nu}}{dz_h} &= \sum_q \int_{z_h}^1 \frac{dz}{z} D_{q \rightarrow h}(z_h/z) f_q(x_B) \int dY^- \int d\delta y^- \frac{4}{l_T^A} \\ &\times \int d^2 l_T \frac{\alpha_s}{2\pi} C_A \frac{1+z^2}{1-z} \frac{2\pi\alpha_s}{N_C} H_{\mu\nu}^{(0)} e^{-i(x_L+x_D)p^+ \delta y^-} \\ &\times (1 - e^{-i(x_L + \frac{x_d}{1-z})p^+(Y^- - \frac{\delta y^-}{2})}) (1 - e^{i(x_L + \frac{x_d}{1-z})p^+(Y^- - \frac{\delta y^-}{2})}) \\ &\times \langle A | F_\sigma^+(Y^- + \frac{\delta y^-}{2}) F^{+\sigma}(Y^- - \frac{\delta y^-}{2}) | A \rangle . \end{aligned} \quad (3.13)$$

Where

$$\begin{aligned} x_L &= \frac{l_T^2}{2p^+ q^- z(1-z)} , \\ x_D &= \frac{k_T^2 - 2\vec{k}_T \cdot \vec{l}_T}{2p^+ q^- z} , \end{aligned} \quad (3.14)$$

l_T is the transverse momentum of the radiated gluon, k_T is the initial quark's transverse momentum, and $z = l_q^-/q^-$ is the momentum fraction of the outgoing quark. Also, C_A is the color factor associated with gluon emission from a gluon and N_C is the number of colors.

The terms in the third line of eq. 3.13,

$$(1 - e^{-i(x_L + \frac{x_D}{1-z})p^+(Y^- - \frac{\delta y^-}{2})})(1 - e^{i(x_L + \frac{x_D}{1-z})p^+(Y^- - \frac{\delta y^-}{2})}), \quad (3.15)$$

after taking $x_L + \frac{x_D}{1-z} \simeq x_L$ since $x_D \ll x_L$, simplify to $2 - 2\cos(x_L P^+ Y^-)$.

Then defining

$$\hat{q}(Y^-) = \int \frac{d\delta y^-}{2\pi} \frac{4\pi\alpha_s}{N_C} e^{-i(x_L + x_D)p^+\delta y^-} \langle A | F_\sigma^+(Y^- + \frac{\delta y^-}{2}) F^{+\sigma}(Y^- - \frac{\delta y^-}{2}) | A \rangle \quad . \quad (3.16)$$

The hadronic tensor then becomes

$$\frac{dW^{\mu\nu}}{dz} = \sum_q \int \frac{dz_h}{z} D_{q \rightarrow h}(z_h/z) f_q(x_B) P(\frac{z_h}{z}, z). \quad (3.17)$$

In this equation, $P(\frac{z_h}{z}, z)$ represents the probability of the quark dropping to a momentum fraction in the range of z and $z + \delta z$ and afterwards fragmenting into a hadron with momentum fraction between y and δy . In this case, $y = z_h/z$.

The expression for $P(\frac{z_h}{z}, z)$ is then

$$P(\frac{z_h}{z}, z) = \int dY^- \hat{q}(Y^-) \int dl_T^2 \frac{\alpha_s}{2\pi} C_A \frac{1+z^2}{1-z} H_{\mu\nu}^{(0)} \frac{4}{l_T^4} (2 - 2\cos(x_L P^+ Y^-)). \quad (3.18)$$

The energy lost to the emitted gluon is then $q^-(1-z)P(z)dz$ in the single scattering single emission regime.

To calculate energy loss in the multiple scattering single emission regime, the single scattering single emission kernel was iterated [83] using a Dokshitzer-Gribov-Lipatov-Altarelli-Parisi (DGLAP) equation [92][93][94][95].

In the absence of a medium [96],

$$\frac{\delta D_q^h(z, Q^2)}{\delta \ln(Q^2)} = \frac{\alpha_s(Q^2)}{2\pi} \int_z^1 \frac{dy}{y} P_{q \rightarrow i}(y) D_i^h\left(\frac{z}{y}, Q^2\right). \quad (3.19)$$

With medium corrections included [96],

$$\frac{\delta D_q^h(z, Q^2, q^-)|_{\xi_i}^{\xi_f}}{\delta \ln(Q^2)} = \frac{\alpha_s}{2\pi} \int_z^1 \frac{dy}{y} \int_{\xi_i}^{\xi_f} d\xi \tilde{P}(y) K_{q^-, Q^2}(y, \xi) D_q^h\left(\frac{z}{y}, Q^2, q^-, y\right)|_{\xi}^{\xi_f} \quad (3.20)$$

where the scattering kernel $K_{q^-, M^2}(y, \xi)$ is

$$K_{q^-, M^2}(y, \xi) = \frac{2\pi\alpha_s\rho(\xi)}{N_C} \left[2 - 2\cos\left\{ \frac{M^2(\xi - \xi_i)}{2q^-y(1-y)} \right\} \right]. \quad (3.21)$$

In Eqs. 3.20 and 3.21 ξ denotes the location of the scattering vertex of the hard parton off the medium and $\rho(\xi)$ is the gluon density at ξ in the medium.

This formulation is used in the MATTER event generator code to perform jet energy loss, described in the next section.

3.3 Phenomenology of Jet Energy Loss

The initial state of the simulation begins in two parts: PYTHIA and the OSU hydrodynamic simulation iEBE-VISHNU. The hard parton from PYTHIA and the medium from the hydrodynamic simulation were then read by the MATTER event generator for jet showering. The MATTER event generator was used to simulate jet showering in both vacuum and in medium. While the parton showers generated by MATTER could be used with a hadronization scheme, such as the recombination code from Texas A&M [97][98] for hadronic results, the majority of the results presented in further sections were instead performed by generating partonic spectra and using the Kniehl-Kramer-Potter (KKP) fragmentation function[99] to generate leading hadron spectra. Some earlier analyses used the earlier Binnewies-Kniehl-Kramer (BKK) fragmentation function [100][101], however all of these were redone using the later KKP fragmentation function. In addition, FastJet[102][103]

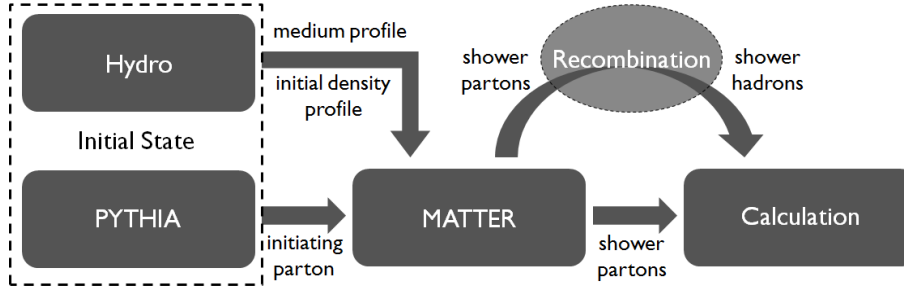


Figure 3.1: Code flowchart showing data input/output for each code set

was run over the generated partonic showers to generate full jets using the anti- k_T algorithm with an $R = 0.4$ for analysis. A general flowchart of this simulation is shown in Fig. 3.1.

3.3.1 Generating the Initiating Hard Parton using PYTHIA

PYTHIA was used to generate the initial hard parton for the shower. Nuclear shadowing was not included, but is a planned future modification. PYTHIA was setup with the center-of-mass energy of the collision and the p_T bounds for the hard process as well as turning off final state radiation and all hadron level processes. For each of the produced events, the leading two partons at midrapidity ($y \leq \pm 0.25$) were used for jet quenching. Multiple hard- p_T bins were used to enhance statistics for high p_T values ($\geq 5 GeV$) to compensate for the falling jet spectrum. An example of this is shown in Fig. 3.2 where the spectrum for charged hadrons from a p - p collision is shown for LHC energies. The cross-section for each of these bins was recorded from PYTHIA for use in the subsequent calculations to determine simulation results.

3.3.2 Hydrodynamic Simulation of the QGP

The OSU hydrodynamic code "iEBE-VISHNU" (Event-By-Event Viscous Israel Stewart Hydrodynamics aNd UrQMD) is an event-by-event 2+1d hydrodynamic simulation of the QGP in relativistic heavy-ion collisions with fluctuating initial conditions. This package performs this simulation utilizing the Israel-Stewart formulation [104][105][106]; this particular formulation explicitly includes causality as opposed to the previous attempts using the Navier-Stokes equation [107] [108] which were not successfully applied to relativistic systems.

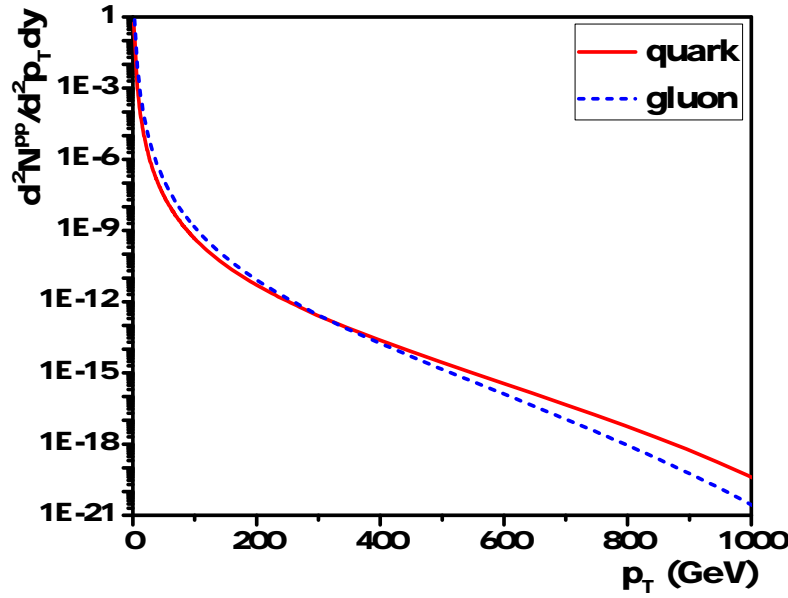


Figure 3.2: Plot showing the output spectra of quarks and gluons from PYTHIA for a LHC p - p event, performed using the procedure described in section 3.3.1.

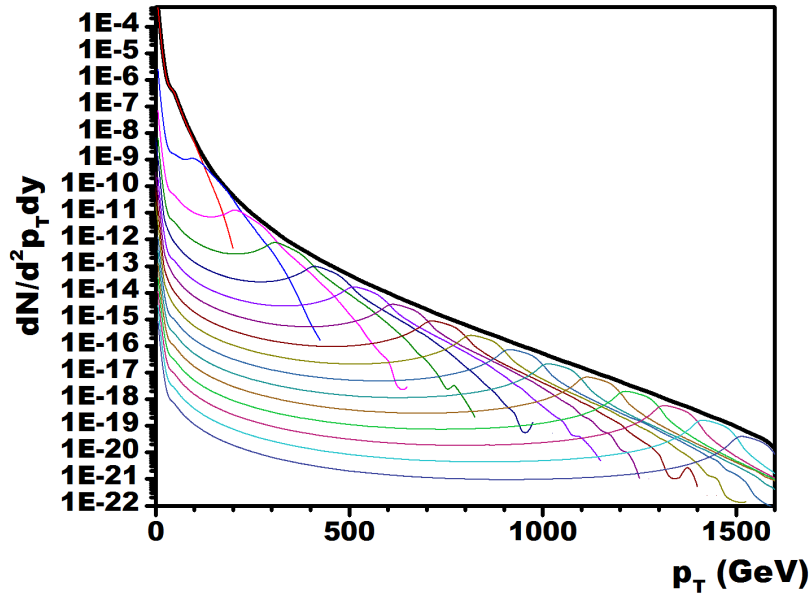


Figure 3.3: Plot showing the contributions of each hard p_T bin to the sum of produced charged hadrons in a LHC p - p event.

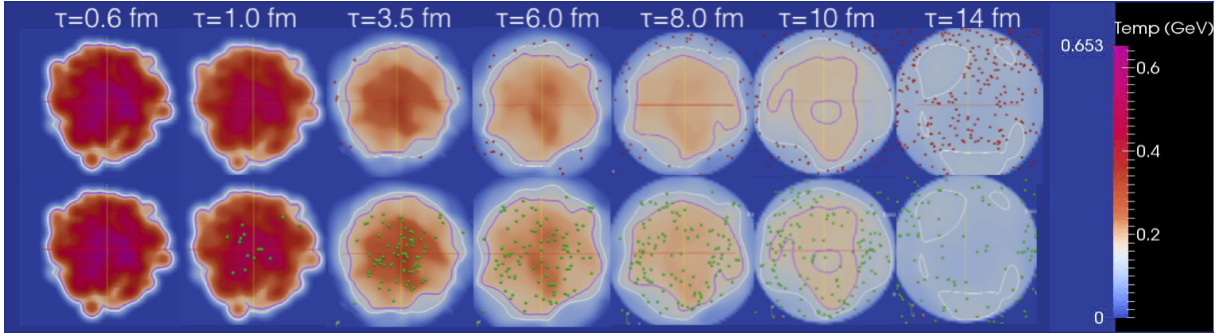


Figure 3.4: An example event produced from the OSU iEBE-VISHNU hydrodynamic simulation (Taken from <https://u.osu.edu/vishnu/physics/>).

Also, this simulation includes the UrQMD (Ultrarelativistic Quantum Molecular Dynamics) model [25][26]; though the hadrons produced from this model, while an integral part of the hydrodynamic code package, were not used in this study. This simulation is used to model the collision after thermal equilibrium is established, whereas work has been done to study the effects in the pre-equilibrium state in [18][109][110][111], though these effects have not been incorporated in this study. It was used to generate both a medium for jet quenching (an evolving entropy density profile) and to report the initial density profile $T_{AA}(x, y)$ for sampling the hard parton's initial location. While it could have been used to generate thermal partons and/or hadrons for the background of the jet, this was not performed for this analysis though it is a planned future endeavor. An example of the evolution of an event is shown in Fig 3.4.

3.3.3 The MATTER Event Generator

The jet quenching portion of the simulation was performed with the MATTER++ (Modular All Twist Transverse scattering based Energy-loss Routines in C++) event generator [88]. It is based on the Higher-Twist formalism [88] and as such it is primarily applicable to the high energy, high virtuality portion of a particular jet in the 'few' scatterings (meaning zero to one) per emission limit. In this regime, light quark modification is sensitive to the high Q^2 , low- x part of the in-medium gluon distribution. In order to introduce space-time into the shower, the notion that the uncertainty in the momentum is conjugate to the posi-

tion (and likewise, that the uncertainty in the position is conjugate to the momentum) was used. For a reasonable uncertainty, it is asserted that $\delta q^+ \ll q^+$. Then there is an assumed Gaussian distribution around q^+ and it is insisted that

$$\langle \tau \rangle = 2q^-/Q^2. \quad (3.22)$$

Then to obtain the z^- a δq^+ distribution is assumed. Thus, it is obtained that:

$$\rho(\delta q^+) = \frac{\exp\left[-\frac{(\delta q^+)^2}{2[2(q^+)/\pi]}\right]}{\sqrt{2\pi[2(q^+)^2/\pi]}}. \quad (3.23)$$

The off-shell quark will have momentum $q = [q^-, q^+, 0, 0]$. This allows for the parton's travel length to the next split to be determined.

Before the length traversed for the current parton can be calculated however, its virtuality must first be determined. This is done by sampling the Sudakov form factor to obtain the maximum virtuality μ^2 (which is also the running scale) of the splitting parton, which is constructed as:

$$S_\xi(Q_0^2, Q^2) = \exp\left[\int_{2Q_0^2}^{Q^2} \frac{d\mu^2}{\mu^2} \frac{\alpha_s(\mu^2)}{2\pi} \cdot \int_{Q_0/Q}^{1-Q_0/Q} dy P_{qg}(y) \left\{1 + \int_{\xi_i^-}^{\xi_i^- + \tau^-} d\xi K_{p^-, \mu^2}\right\}\right]. \quad (3.24)$$

The Sudakov itself gives the probability of the parton having no emission from initial virtuality $2Q_0$ to final virtuality Q . $P_{qg}(y)$ is the splitting function for a quark to split into a quark and a gluon where the final quark carries momentum yq^- and the gluon carries momentum $(1-y)q^-$. The single emission, multiple scattering kernel K as a function of the momentum fraction y and the location of the parton ξ starting from location ξ_i is:

$$K_{p^-, \mu^2}(y, \xi) = \frac{2\hat{q}}{\mu^2} \left[2 - 2\cos\left\{\frac{\mu^2(\xi - \xi_i)}{2p^-y(1-y)}\right\}\right], \quad (3.25)$$

where \hat{q} is the jet transport coefficient [112][113]. This kernel was discussed in the previous

section 3.2 where it was derived by Guo and Wang [89][90]. Another formula for the kernel was derived by Aurenche, Zakharov, and Zaraket [114][115] which includes additional terms that were ignored by Guo and Wang. This kernel could have been used instead, but the results generated in this study used the Guo and Wang kernel.

Since this simulation is based on the Higher-Twist scheme, multiple emissions are ordered in p_T . These ordered multiple emissions are only considered when the multiple soft scatterings mildly effect the virtuality of the parent parton. For partons where the virtuality has become too low, this calculation is no longer applicable. This means that this procedure is only valid while:

$$\frac{\hat{q}\tau}{\mu^2} \lesssim 1 \quad . \quad (3.26)$$

With this, the code can read in a high- p_T parton, that was generated using PYTHIA, and begin to generate the shower. In order to do so the entropy density of the medium is read in from the pre-run hydrodynamic simulation. This is used to modify \hat{q} in the Sudakov form factor. The Sudakov is sampled to return the largest virtuality allowable for the process. This virtuality is then used to determine the distance traveled by the parton before it splits. The splitting function is sampled to determine the momentum fraction y of one of the outgoing partons. This process is repeated over the outgoing partons for each iteration until all the generated partons have a virtuality at or less than 1 GeV^2 , beyond which the Higher Twist formalism is no longer applicable.

The final partons in the shower are then checked to determine if they are able to escape the medium; this is done by removing any parton that is further than 1 fm from the edge of the medium. This can remove high energy but low virtuality partons, though this is a rare occurrence; instead a planned method to deal with these partons is by handing them off to an event generator that includes a multiple scatterings per emission treatment, such as MARTINI [65]. The low energy, low virtuality partons that were removed are planned to be used to generate source terms for a medium response to the jet. The partons that escape the medium are then taken as the final generated shower from the MATTER code.

3.4 Results and Experimental Comparison

With the model described in the earlier sections constructed to simulate jet production in heavy-ion events, results were generated to compare to expected and experimental results. Events were simulated over a range of hard p_T bins: 2.5-52.5 GeV in 5 GeV wide bins for Au+Au collisions and 2.5-227.5 GeV for Pb+Pb collisions. The partons produced in the shower after the MATTER event generator was used to simulate the jet were then either used to perform jet analyses with FastJet, or used directly to construct quark and gluon spectra. To determine the nuclear modification factor R_{AA} , the calculation started by taking each of these hard p_T bins, weighting it by its corresponding p - p cross-section, then summing over all the aforementioned hard p_T bins to get the total spectra for either quarks and gluons or for jets. The nuclear modification factor R_{AA} is defined as

$$R_{AA} = \frac{\int_{b_{min}}^{b_{max}} d^2b \frac{d^4 N_{AA}}{d^2 p_T dy d^2 b}}{\langle N_{bin}(b_{min}, b_{max}) \rangle \frac{d^3 N_{pp}}{d^2 p_T dy}}, \quad (3.27)$$

where N is the yield of jets or leading hadrons binned in p_T and rapidity. The numerator in the preceding formula also includes an integral over a range of the impact parameter b to construct bins in centrality. The factor $\langle N_{bin}(b_{min}, b_{max}) \rangle$ is the mean number of binary nucleon-nucleon collisions N_{bin} of a nuclear collision from a given centrality bin for $b_{min} < b < b_{max}$. This gives a method of quantifying nuclear effects, as it allows for a comparison of heavy-ion data where the QGP was created to p - p events where we do not expect the presence of the QGP or other nuclear influences such as initial state cold nuclear matter effects.

The A - A cross-section in this case is just N_{bin} multiplied by the previous p - p cross-section. The KKP fragmentation function was applied to partonic spectra to obtain leading hadron (or pion) spectra, which were then used to calculate R_{AA} as mentioned above. The results of these calculations are given in Figs 3.5, 3.6, and 3.7. These results use a $\hat{q}_0 = 2.4 \text{ GeV}^2 / fm$

except for leading hadron data from Au+Au collisions; \hat{q}_0 is the value of \hat{q} at the center of an averaged 0-5% centrality bin Au+Au collision.

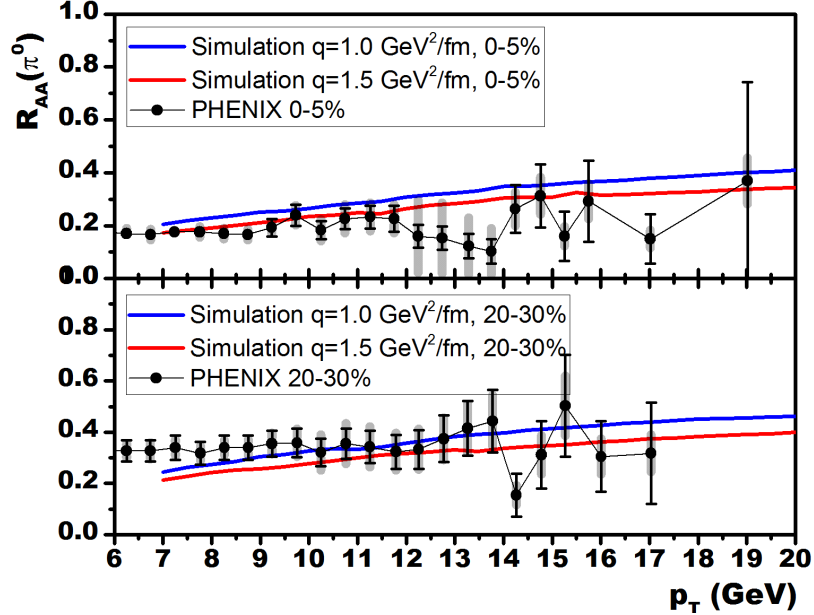


Figure 3.5: Leading pion R_{AA} for 200 GeV Au+Au compared to PHENIX data [9] for varying \hat{q}_0

While v_2 measurements were not calculated, an in-plane vs. out-of-plane simulation was carried out for a medium with a smooth, static density profile, as a first step in determining the effects of an anisotropic medium. These were plotted for a medium representative of the "average" medium for 20-30% centrality Au+Au events with a hard p_T bin of 12.5-17.5 GeV at the parton level (for both quarks and gluons) in Fig. 3.8. Strictly speaking this is not an R_{AA} as it was only determined for a single hard p_T bin, but should be indicative of a complete in-plane vs. out-of-plane R_{AA} calculation. This plot is shown in Fig. 3.8. It should be noted that the observed behavior of the out-of-plane ratio being more suppressed than the in-plane ratio is consistent with naive expectation, and the magnitude of the effect of approximately 0.3-0.5 is entirely reasonable considering the somewhat unrealistic medium.

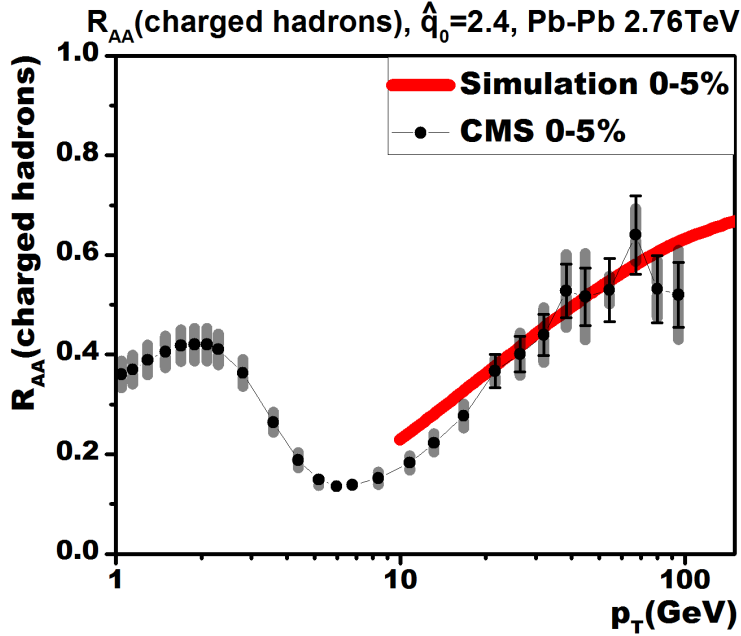


Figure 3.6: Leading hadron R_{AA} for 2.76 TeV Pb+Pb 0-5% centrality compared to CMS data [10] with $\hat{q}_0 = 2.4 \text{ GeV}^2/\text{fm}$

3.4.1 Integration of the Texas A&M Recombination Code

While there were no results calculated using the Texas A&M recombination code that were compared to experiment, there has been some work done in order to integrate it with the simulation as a whole. The dN/dp_T histogram was calculated for a 100 GeV quark jet both in vacuum and in a 4 fm brick. The KKP fragmentation function was applied to the quark and gluon histograms, while the recombination code was used on an event-by-event basis to generate pions from the partons in the event to be histogrammed. The results of this procedure are shown in Fig. 3.9 for both the KKP fragmentation function and the recombination code in addition to the raw quark and gluon histograms.

Also, to compare the two methods of calculating hadron spectra, pion spectra from both the KKP fragmentation function and the recombination code were calculated. The medium used was generated using the OSU hydrodynamic simulation of a 0-5% Au+Au collision. The data from the KKP fragmentation function were calculated in the same way as described in

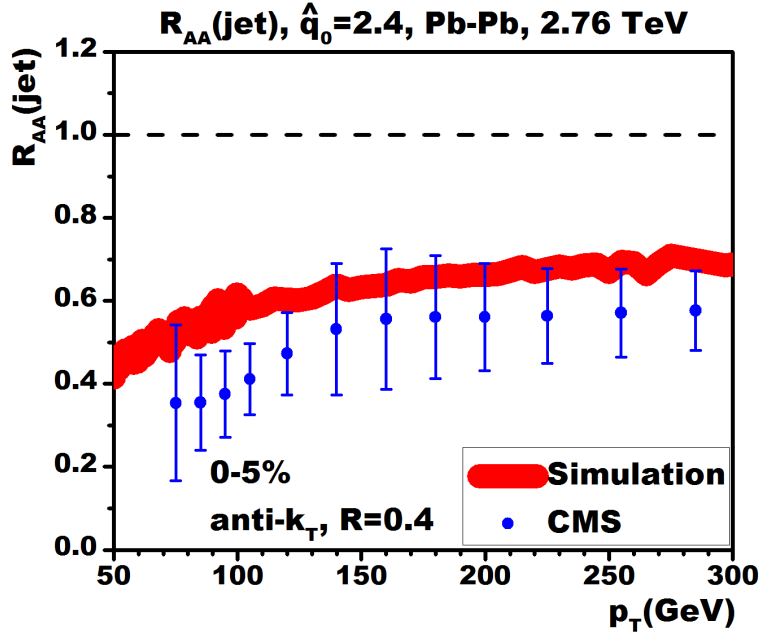


Figure 3.7: Jet R_{AA} for 2.76 TeV Pb+Pb 0-5% centrality compared to CMS data [11] with $\hat{q}_0 = 2.4 \text{ GeV}^2/fm$

the above text, whereas the data using the recombination code were generated by applying the recombination code over each of the events produced for each of the hard p_T bins. The hadrons produced were then histogrammed and the calculation to determine the spectra proceeded similarly to the parton spectra before. The spectra, and R_{AA} calculated from these spectra, were determined for pion production, and the results are given in Figs. 3.10 and 3.11.

3.5 Discussion

In this work the development of a Monte-Carlo event generator for jet quenching based on the HT scheme was discussed. The designed event generator was constructed in several sections. The initial state of the heavy-ion collision was built using PYTHIA to generate the hard parton and the OSU Hydrodynamic simulation to generate the medium. The jet shower was simulated using the MATTER event generator. This shower was then used for subsequent calculations; using either the KKP fragmentation function for hadronic results

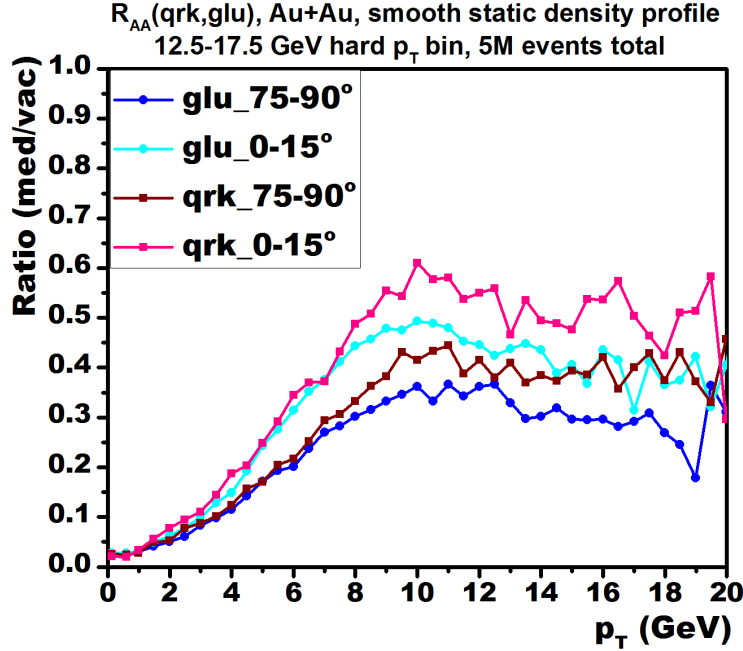


Figure 3.8: A plot of the ratio of the in-medium to vacuum production of quarks in gluons in a smooth static medium representative of Au+Au collisions for in-plane vs. out-of-plane results.

or FastJet running with the anti- k_T algorithm to construct partonic jet observables.

The results produced from these simulations are consistent with R_{AA} hadronic experimental data at both RHIC and the LHC. The agreement between the simulated and experimental data indicates a measure of success in the construction of this event generator. In addition some future feature implementations were tested in the form of preliminary analyses (in the form of in-plane vs. out-of-plane results) and inclusion of the Texas A&M recombination code results and comparisons to the current method of calculating hadron production both were shown to behave as anticipated. This fact bodes well for future enhancements of this work. The analysis is by no means exhaustive as there a number of analyses possible that have not yet been completed and there are a number of improvements that yet remain to be added.

In the future, we intend to further refine the presented results. We also plan to present further analyses including v_2 and jet shapes. Further refinements include a method of han-

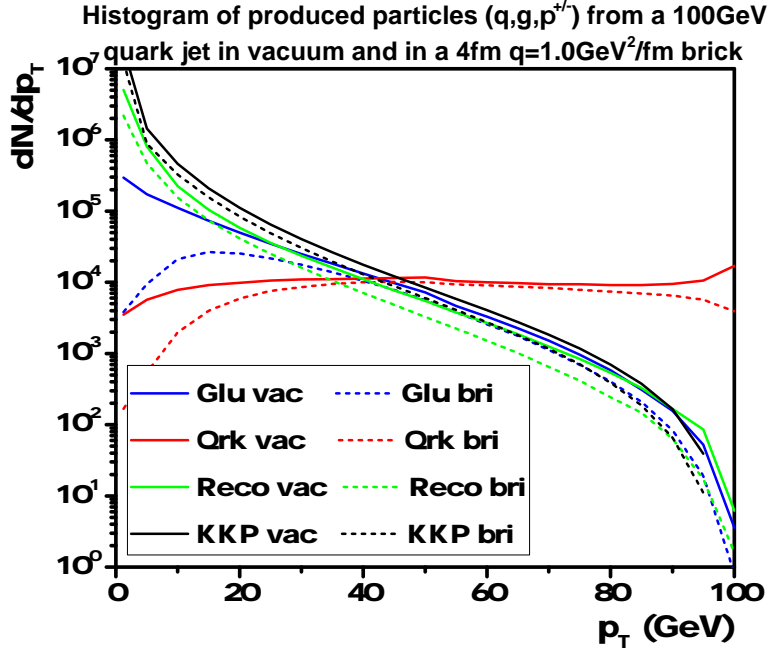


Figure 3.9: A dN/dp_T histogram plotted for a 100 GeV quark jet in vacuum and in a 4 fm $\hat{q} = 1.0\text{GeV}^2/\text{fm}$ brick for pion production determined by the KKP fragmentation function and the Texas A&M recombination code, as well as for raw quark and gluon production.

dling partons with a virtuality of 1 GeV or less, incorporating medium response via a source term, including thermal hadrons, further incorporating the Texas A&M recombination code, and including thermal-shower recombination hadrons. With the execution of these plans there is hope to see even better agreement with experimental data, to compare to more experimental data, and to predict a number of future experimental results.

This development of the event generator constructed in this work has allowed for the simulation of jet observables based on the HT scheme to be compared to experimental data. Future studies with this event generator, as well as planned future enhancements to it, will hopefully reveal new information about heavy-ion collisions in general, and the QGP specifically. The current work represents a step in this direction, giving insight into the potential knowledge to be gained in this pursuit.

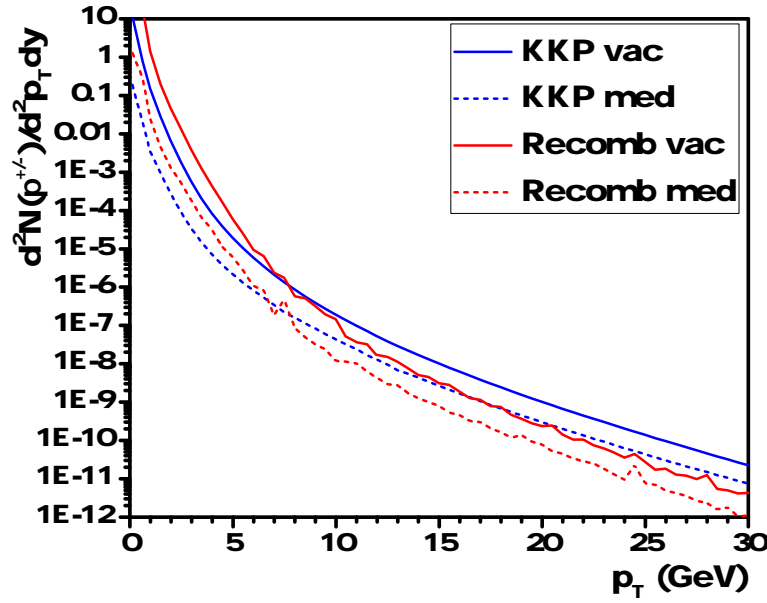


Figure 3.10: A plot of pion spectra generated using the KKP fragmentation function and the Texas A&M recombination code for vacuum jets and for 0-5% 200 GeV Au+Au collisions.

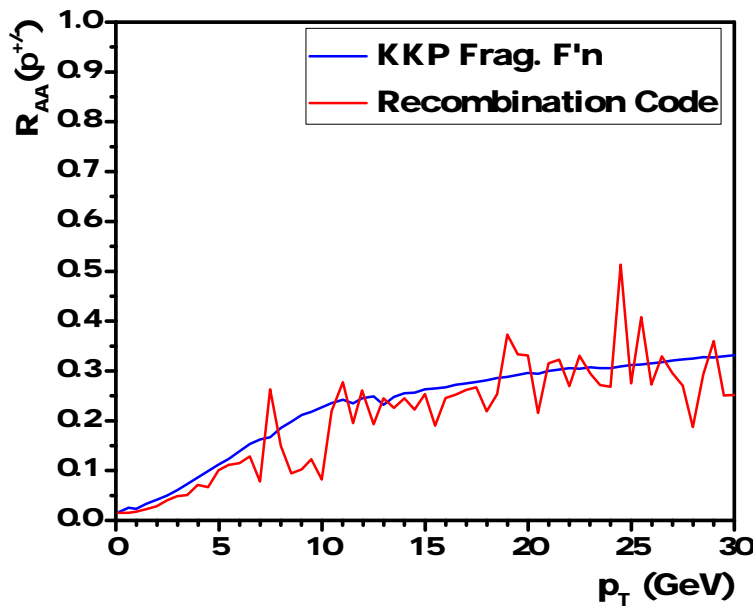


Figure 3.11: Leading pion R_{AA} for 0-5% 200 GeV Au+Au events, generated by using the KKP fragmentation function and by using the Texas A&M recombination code.

CHAPTER 4: SUMMARY AND DISCUSSION

4.1 Summary

In this work, Monte-Carlo event generators were developed to study nuclear effects in heavy-ion collisions. Initial state effects were studied in $d(p)$ - A collisions and simulations where the production of a QGP is not expected, and final state effects were studied in A - A collisions and simulations where the QGP is expected to be produced. These effects were studied via jet modification within the systems of interest.

The $d(p)$ - A simulation was used to study centrality dependent jet modification with interesting behavior seen with experimental results from both RHIC and the LHC. Specifically, the naive expectation is for jet production in central events to show maximal nuclear modification and for production in peripheral events to show minimal modification. In essence, peripheral events are expected to behave as a superposition of p - p events, whereas if any nuclear effects are present they are expected to show predominantly in central events. However, the experimental results seemed to indicate the exact opposite; jet production in central events were behaving as if they were just a superposition of p - p events and production in peripheral events were showing significant nuclear effects.

The construction of the simulation was built on an altered version of PYTHIA, which has widespread use as a p - p event generator. These alterations involved the modification of the PDF calls within the PYTHIA code in order to run proton-superproton events, so that a p - A collision could be simulated in such a manner that the event was run without resampling the PDF. Current event generators treat these events by running N p - p events, however, this is an unphysical method as the PDF in the impacting nucleon is time dilated to the extent that it's PDF does not fluctuate over the event. When events with jet production are observed, the PDF must preexist in a configuration with a high x "hard" parton. This means that there is less energy available in the nucleon to produce low x "soft" partons, and thus soft hadron production is suppressed in these events. Since, experimentally, events are binned in centrality by soft particle production (N_{chg} deposited in the forward detector), this leads to

those events being placed in more peripheral bins than if they could have been binned by the number of binary collisions N_{bin} . In the simulation, however, both the N_{bin} and N_{chg} for a given event is available. This allowed for the binning of events by either. Binning by N_{bin} showed results that were inconsistent with experimental results, but did conform to naive expectations. Binning by N_{chg} on the other hand showed results that were consistent with experimental results at both RHIC and the LHC.

The construction of an A - A simulation was used to study jet modification in full heavy-ion collisions. Specifically, the study of jet suppression due to the presence of the QGP. There are a number of preexisting simulations, but this particular construction is one of the first to include a space-time structure of the shower that interacts with a space-time dependent medium on an event-by-event basis. The simulation was constructed in several parts; the p - p event generator PYTHIA, the OSU hydrodynamic simulation iEBE-VISHNU, and the MATTER++ jet showering event generator being the primary components. PYTHIA was used to generate the initial high p_T hard parton to start the jet shower. iEBE-VISHNU was used to generate the medium of the collision, as well as to provide an initial density profile for that event to sample for the jet starting location within the event. The MATTER event generator used the initiating partons produced using PYTHIA and generated the jet shower within the medium profile produced using iEBE-VISHNU, in addition to producing showers without a medium for vacuum results. The parton showers produced using MATTER could be used as direct input to calculate partonic observables. One could also calculate hadronic observables using either the KKP fragmentation function or the Texas A&M recombination code.

The output of these procedures was used for several calculations of interest, including spectra and ultimately R_{AA} . Experimental comparisons were performed with the KKP fragmentation function and the R_{AA} calculated from the simulation shows strong agreement with the experimental results at both RHIC and the LHC. In addition, a plot of the angular dependence of the ratio of in-medium to vacuum production of quarks and gluons showed

expected behavior. Also, the implementation of the Texas A&M recombination code showed reasonable and anticipated results when compared to the results using the KKP fragmentation function for pion production in a brick with a fixed initial parton energy, pion spectra at RHIC energies, and R_{AA} at RHIC energies.

4.2 Discussion

The simulations constructed were used to examine both initial state and final state nuclear effects. The p - A events provide a baseline for the full A - A events so that any effects due to the QGP can be isolated. The results generated by both simulations exhibited effects that were either physically expected or were outright consistent with experimental results at both RHIC and the LHC. In $d(p)$ - A collisions, an interesting centrality dependent jet production effect was explained with energy conservation; events that produce a jet have less energy available for soft particle production. Thus when an event is binned in centrality by soft charged particle production, events with a jet tend to fall into more peripheral bins since those events produce less charged particles than would have been present in the event if there had not been a jet. In A - A collisions, the simulation was able to generate R_{AA} consistent with experimental measurements at both RHIC and the LHC, showing the practicality of this event generator. In addition, results were also produced for a smooth static medium representative of a 20-30% centrality Au-Au collision where the ratio of in-medium to vacuum jet production showed reasonable angular dependence. Also, comparisons were generated using the KKP fragmentation function (which had been used to generate all hadronic results for experimental comparison) and the Texas A&M recombination code, which showed reasonable agreement. As this recombination code is expected to be integrated into the simulation proper, this agreement is indicative of a successful inclusion of this code and the expectation of the generation of accurate future results.

While there is remarkable agreement for most experimental data compared to from these simulations, there are a few caveats that need to be addressed. For the $d(p)$ - A simulation, there is concern with the shape of the charged hadron R_{CP} data compared to the experi-

ment; while the magnitude of the suppression was captured for large p_T the shape was not. This discrepancy could be due to the increased color connections available to the produced hard parton in this formulation as compared to what it would actually have in practice; in this formulation the parton is able to form color connections to any of the nucleons in the "superproton" whereas in actuality it should only have a color connection to the generating nucleon only. We did not study this effect, but its influence could explain the shape of the simulation results. Also, in this simulation the production of soft hadrons is different than in experiment; the production of these should be performed with an energy-enhanced PDF, however this leads to a severe overproduction of high-x partons. This lead to just a 'number of nucleons present' enhancement of the "superproton" PDF in order to preserve the jet production cross-section. For the A - A simulation, there are a number of experimental results yet to be compared such as jet v_2 , and a number of physics effects that need to be included. The simulation needs a method of handing partons that have a virtuality less than 1 GeV, it needs the inclusion of a medium response to the jet, it needs the inclusion of thermal partons, and the complete integration of the Texas A&M recombination code into the simulation itself needs to be done.

Future work with these simulations involves the mitigation if not correction of these issues. The $d(p)$ - A event generator needs a revamped PDF sampling routine which will likely not be able to be performed using PYTHIA. The A - A event generator is slated to incorporate a number of physics features including a method of handing low virtuality (≤ 1 GeV) high-energy partons, the incorporation of a medium response via a source term in the hydrodynamic simulation, the inclusion of thermal partons from the hydro, and the integration of the Texas A&M recombination code. The incorporation of these fixes will allow for more experimental comparisons to be performed, and to be done with better accuracy.

While the implementation of these fixes and enhancements represents a large undertaking, the current work presented here is a marked step in the direction of gaining new insight into constructing Monte-Carlo event generators to simulate heavy-ion collisions. Both in the

fact that this work has shown the feasibility of incorporating novel approaches to simulating heavy-ion collisions and the success in reproducing experimental results, but also in providing information as to the construction necessary for future event generators. The work presented here demonstrates a study in these simulations that quantify nuclear effects, ranging from effects due to the nuclear initial state in $d(p)$ - A collisions to studying the final state in A - A collisions with the presence of the QGP. These simulations represent a new tool to examine features in heavy-ion collisions and provides a potential base for the development of future, more sophisticated, event generators.

BIBLIOGRAPHY

- [1] J. Pumplin et al., JHEP **07**, 012 (2002).
- [2] H. Song, S. A. Bass, and U. Heinz, Phys. Rev. **C83**, 054912 (2011), [Erratum: Phys. Rev.C87,no.1,019902(2013)].
- [3] B. I. Abelev et al., Phys. Rev. **C77**, 054901 (2008).
- [4] K. Aamodt et al., Phys. Rev. Lett. **105**, 252302 (2010).
- [5] B. Sahlmueller, Nucl. Phys. **A904-905**, 795c (2013).
- [6] A. Adare et al., (2015).
- [7] G. Aad et al., Phys. Lett. **B748**, 392 (2015).
- [8] T. A. collaboration, (2014).
- [9] A. Adare et al., Phys. Rev. **C87**, 034911 (2013).
- [10] S. Chatrchyan et al., Eur. Phys. J. **C72**, 1945 (2012).
- [11] V. Khachatryan et al., Phys. Rev. **C96**, 015202 (2017).
- [12] The Durham HepData Project: PDF Plotter, <http://hepdata.cedar.ac.uk/pdf/pdf3.html>, 2017.
- [13] P. Huovinen and P. V. Ruuskanen, Ann. Rev. Nucl. Part. Sci. **56**, 163 (2006).
- [14] D. Teaney, Phys. Rev. **C68**, 034913 (2003).
- [15] T. Hirano and M. Gyulassy, Nucl. Phys. **A769**, 71 (2006).
- [16] L. P. Csernai, J. Kapusta, and L. D. McLerran, Phys. Rev. Lett. **97**, 152303 (2006).
- [17] P. Kovtun, D. T. Son, and A. O. Starinets, Phys. Rev. Lett. **94**, 111601 (2005).
- [18] S. Gavin, G. Moschelli, and C. Zin, Phys. Rev. **C95**, 064901 (2017).
- [19] C. Shen et al., Comput. Phys. Commun. **199**, 61 (2016).
- [20] C. M. Hung and E. V. Shuryak, Phys. Rev. **C57**, 1891 (1998).

- [21] D. A. Teaney, Viscous Hydrodynamics and the Quark Gluon Plasma, in *Quark-gluon plasma 4*, edited by R. C. Hwa and X.-N. Wang, pages 207–266, 2010.
- [22] D. Teaney, J. Lauret, and E. V. Shuryak, (2001).
- [23] P. Romatschke and M. Strickland, *Phys. Rev.* **D68**, 036004 (2003).
- [24] Z. Fodor, S. D. Katz, and K. K. Szabo, *Phys. Lett.* **B568**, 73 (2003).
- [25] S. A. Bass et al., *Prog. Part. Nucl. Phys.* **41**, 225 (1998).
- [26] M. Bleicher et al., *Journal of Physics G: Nuclear and Particle Physics* **25**, 1859 (1999).
- [27] P. Arnold, G. D. Moore, and L. G. Yaffe, *JHEP* **11**, 001 (2000).
- [28] P. B. Arnold, G. D. Moore, and L. G. Yaffe, *JHEP* **05**, 051 (2003).
- [29] P. B. Arnold, G. D. Moore, and L. G. Yaffe, *JHEP* **01**, 030 (2003).
- [30] S. Turbide, R. Rapp, and C. Gale, *Phys. Rev.* **C69**, 014903 (2004).
- [31] S. Turbide, C. Gale, S. Jeon, and G. D. Moore, *Phys. Rev.* **C72**, 014906 (2005).
- [32] J. C. Collins, D. E. Soper, and G. Sterman, *Phys. Lett.* **B134**, 263 (1984).
- [33] J. C. Collins, D. E. Soper, and G. Sterman, *Nucl. Phys.* **B261**, 104 (1985).
- [34] J. C. Collins, D. E. Soper, and G. Sterman, *Nucl. Phys.* **B308**, 833 (1988).
- [35] G. Sterman and S. Weinberg, *Phys. Rev. Lett.* **39**, 1436 (1977).
- [36] S. D. Ellis and D. E. Soper, *Phys. Rev.* **D48**, 3160 (1993).
- [37] M. Cacciari, G. P. Salam, and G. Soyez, *JHEP* **04**, 063 (2008).
- [38] C. Adler et al., *Phys. Rev. Lett.* **90**, 082302 (2003).
- [39] S. S. Adler et al., *Phys. Rev. Lett.* **91**, 072303 (2003).
- [40] S. S. Adler et al., *Phys. Rev.* **C75**, 024909 (2007).
- [41] S. Adler et al., *Phys.Rev.Lett.* **98**, 172302 (2007).
- [42] M. G. Wysocki, *Nucl.Phys.* **A904-905**, 67c (2013).

- [43] D. V. Perepelitsa, Centrality and rapidity dependence of inclusive jet production in $\sqrt{s_{NN}} = 5.02$ TeV p +Pb collisions with the ATLAS detector, Technical Report ATLAS-PROC-2014-095, CERN, Geneva, 2014.
- [44] T. Sjöstrand et al., *Comput. Phys. Commun.* **191**, 159 (2015).
- [45] A. Bzdak, V. Skokov, and S. Bathe, (2014).
- [46] M. Alvioli, B. A. Cole, L. Frankfurt, D. V. Perepelitsa, and M. Strikman, (2014).
- [47] N. Armesto, D. C. Gülhan, and J. G. Milhano, *Phys. Lett.* **B747**, 441 (2015).
- [48] X.-N. Wang and M. Gyulassy, *Phys. Rev.* **D44**, 3501 (1991).
- [49] M. Gyulassy and X.-N. Wang, *Comput. Phys. Commun.* **83**, 307 (1994).
- [50] W. Greiner and J. A. Maruhn, *Nuclear models*, Springer, 1996.
- [51] A. Majumder and S. Das Gupta, *Phys. Rev.* **C59**, 845 (1999).
- [52] P. Brussaard and P. Glaudemans, *Shell Model Applications in Nuclear Spectroscopy*, Elsevier, 1977.
- [53] S.-y. Li and X.-N. Wang, *Phys. Lett.* **B527**, 85 (2002).
- [54] T. Sjostrand and M. van Zijl, *Phys. Rev.* **D36**, 2019 (1987).
- [55] S. J. Brodsky, L. Frankfurt, J. F. Gunion, A. H. Mueller, and M. Strikman, *Phys. Rev.* **D50**, 3134 (1994).
- [56] L. Frankfurt, G. A. Miller, and M. Strikman, *Phys. Lett.* **B304**, 1 (1993).
- [57] L. L. Frankfurt and M. I. Strikman, *Phys. Rept.* **160**, 235 (1988).
- [58] A. Beraudo, J. G. Milhano, and U. A. Wiedemann, *Phys. Rev.* **C85**, 031901 (2012).
- [59] N. Armesto, L. Cunqueiro, and C. A. Salgado, *Eur. Phys. J.* **C63**, 679 (2009).
- [60] U. A. Wiedemann, *Nucl. Phys.* **B582**, 409 (2000).
- [61] U. A. Wiedemann, *Nucl. Phys.* **B588**, 303 (2000).
- [62] U. A. Wiedemann, *Nucl. Phys.* **A690**, 731 (2001).

- [63] C. A. Salgado and U. A. Wiedemann, Phys. Rev. **D68**, 014008 (2003).
- [64] N. Armesto, C. A. Salgado, and U. A. Wiedemann, Phys. Rev. **D69**, 114003 (2004).
- [65] B. Schenke, C. Gale, and S. Jeon, (2009).
- [66] P. Arnold, G. D. Moore, and L. G. Yaffe, JHEP **11**, 057 (2001).
- [67] P. Arnold, G. D. Moore, and L. G. Yaffe, JHEP **12**, 009 (2001).
- [68] P. Arnold, G. D. Moore, and L. G. Yaffe, JHEP **06**, 030 (2002).
- [69] G.-Y. Qin et al., Phys. Rev. Lett. **100**, 072301 (2008).
- [70] G.-Y. Qin, J. Ruppert, C. Gale, S. Jeon, and G. D. Moore, (2009).
- [71] M. Gyulassy, P. Levai, and I. Vitev, Nucl. Phys. **B571**, 197 (2000).
- [72] M. Gyulassy, P. Levai, and I. Vitev, Phys. Rev. Lett. **85**, 5535 (2000).
- [73] M. Gyulassy, P. Levai, and I. Vitev, Nucl. Phys. **B594**, 371 (2001).
- [74] M. Gyulassy, P. Levai, and I. Vitev, Phys. Lett. **B538**, 282 (2002).
- [75] M. Djordjevic and M. Gyulassy, Nucl. Phys. **A733**, 265 (2004).
- [76] M. Djordjevic, M. Gyulassy, and S. Wicks, Phys. Rev. Lett. **94**, 112301 (2005).
- [77] K. Zapp, G. Ingelman, J. Rathsman, J. Stachel, and U. A. Wiedemann, Eur. Phys. J. **C60**, 617 (2009).
- [78] K. C. Zapp, F. Krauss, and U. A. Wiedemann, (2012).
- [79] T. Renk, Phys. Rev. **C80**, 044904 (2009).
- [80] T. Renk, (2012).
- [81] I. Lokhtin and A. Snigirev, Eur.Phys.J. **C45**, 211 (2006).
- [82] T. Renk, Phys.Rev. **C79**, 054906 (2009).
- [83] A. Majumder, Phys.Rev. **D85**, 014023 (2012).
- [84] A. Majumder, Phys. Rev. **C80**, 031902 (2009).

- [85] A. Majumder and C. Shen, Phys.Rev.Lett. **109**, 202301 (2012).
- [86] A. Majumder and M. Van Leeuwen, Prog. Part. Nucl. Phys. **66**, 41 (2011).
- [87] A. Majumder and B. Muller, Phys. Rev. **C77**, 054903 (2008).
- [88] A. Majumder, Phys. Rev. **C88**, 014909 (2013).
- [89] X.-F. Guo and X.-N. Wang, Phys. Rev. Lett. **85**, 3591 (2000).
- [90] X.-N. Wang and X.-F. Guo, Nucl. Phys. **A696**, 788 (2001).
- [91] G. S. J.C. Collins, D.E. Soper.
- [92] V. N. Gribov and L. N. Lipatov, Sov. J. Nucl. Phys. **15**, 438 (1972).
- [93] V. N. Gribov and L. N. Lipatov, Sov. J. Nucl. Phys. **15**, 675 (1972).
- [94] Y. L. Dokshitzer, Sov. Phys. JETP **46**, 641 (1977).
- [95] G. Altarelli and G. Parisi, Nucl. Phys. **B126**, 298 (1977).
- [96] A. Majumder, (2009).
- [97] R. J. Fries, K. Han, and C. M. Ko, Nucl. Phys. **A956**, 601 (2016).
- [98] K. C. Han, R. J. Fries, and C. M. Ko, Phys. Rev. **C93**, 045207 (2016).
- [99] B. A. Kniehl, G. Kramer, and B. Potter, Nucl. Phys. **B582**, 514 (2000).
- [100] J. Binnewies, B. A. Kniehl, and G. Kramer, Z. Phys. **C65**, 471 (1995).
- [101] J. Binnewies, B. A. Kniehl, and G. Kramer, Phys. Rev. D **52**, 4947 (1995).
- [102] M. Cacciari, G. P. Salam, and G. Soyez, Eur. Phys. J. **C72**, 1896 (2012).
- [103] M. Cacciari and G. P. Salam, Phys. Lett. **B641**, 57 (2006).
- [104] W. Israel and J. Stewart, Annals of Physics **118**, 341 (1979).
- [105] W. Israel, Annals of Physics **100**, 310 (1976).
- [106] W. Israel and J. Stewart, Physics Letters A **58**, 213 (1976).
- [107] L. D. Landau and E. M. Lifshitz, *Fluid Mechanics*, Oxford, 1963, Sec. 127.

- [108] C. Eckart, Phys. Rev. **58**, 919 (1940).
- [109] S. Gavin and G. Moschelli, Phys. Rev. **C85**, 014905 (2012).
- [110] G. Moschelli and S. Gavin, Nucl. Phys. **A836**, 43 (2010).
- [111] S. Gavin, L. McLerran, and G. Moschelli, Phys. Rev. **C79**, 051902 (2009).
- [112] R. Baier, Nucl. Phys. **A715**, 209 (2003).
- [113] A. Majumder, (2012).
- [114] P. Aurenche, B. G. Zakharov, and H. Zaraket, JETP Lett. **87**, 605 (2008).
- [115] P. Aurenche, B. G. Zakharov, and H. Zaraket, (2008).

ABSTRACT**MONTE-CARLO EVENT GENERATORS FOR JET MODIFICATION IN
 $d(p)$ - A AND A - A COLLISIONS**

by

MICHAEL C. KORDELL II**December 2017**

Advisor: Dr. Abhijit Majumder

Major: Physics

Degree: Doctor of Philosophy

This work outlines methods to use jet simulations to study both initial and final state nuclear effects in heavy-ion collisions. To study the initial state of heavy-ion collisions, the production of jets and high momentum hadrons from jets, produced in deuteron (d)- Au collisions at the Relativistic Heavy-Ion Collider (RHIC) and proton (p)- Pb collisions at the Large Hadron Collider (LHC) are studied as a function of *centrality*, a measure of the impact parameter of the collision. A modified version of the event generator PYTHIA, widely used to simulate p - p collisions, is used in conjunction with a nuclear Monte-Carlo event generator which simulates the locations of the nucleons within a large nucleus. It is demonstrated how events with a hard jet may be simulated, in such a way that the parton distribution function of the projectile is frozen during its interaction with the extended nucleus. Using this approach, it is demonstrated that the puzzling enhancement seen in peripheral events at RHIC and the LHC, as well as the suppression seen in central events at the LHC are mainly due to *mis*-binning of central and semi-central events, containing a jet, as peripheral events. This occurs due to the suppression of soft particle production away from the jet, caused by the depletion of energy available in a nucleon of the deuteron (in d - Au at RHIC) or in the proton (in p - Pb at LHC), after the production of a hard jet. In conclusion, partonic correlations built out of simple energy conservation are responsible for such an effect, though these are sampled at the hard scale of jet production and, as such,

represent smaller states. To study final state nuclear effects, the modification of hard jets in the Quark Gluon Plasma (QGP) is simulated using the Modular All Twist Transverse and Elastic scattering and Radiation (MATTER) event generator. Based on the higher twist formalism of energy loss, the MATTER event generator simulates the evolution of highly virtual partons through a medium. These partons sampled from an underlying PYTHIA kernel undergo splitting through a combination of vacuum and medium induced emission. The momentum exchange with the medium is simulated via the jet transport coefficient \hat{q} , which is assumed to scale with the entropy density at a given location in the medium. The entropy density is obtained from a relativistic viscous fluid dynamics simulation (VISH2+1D) in 2+1 space time dimensions. Results for jet and hadron observables are presented using an independent fragmentation model.

AUTOBIOGRAPHICAL STATEMENT

Name: Michael C. Kordell II

Education:

B.S. Physics, University of West Florida, Pensacola, FL, 2011

A.A., Northwest Florida State College, Niceville, FL, 2008

Professional Experience:

Research Assistant, Wayne State Univ. - Dept. of Physics and Astronomy, Detroit, MI,
01/2013 - current

Teaching Assistant, Wayne State Univ. - Dept. of Physics and Astronomy, Detroit, MI,
08/2011 - 12/2012

Teaching Assistant, Univ. of West Florida - Dept. of Mathematics and Statistics, Pensacola,
FL, 01/2011 - 05/2011

Teacher's Assistant, Univ. of West Florida - Dept. of Mathematics and Statistics, Pensacola,
FL, 09/2010 - 12/2010

Teaching/Research Assistant, Univ. of West Florida - Physics Department, Pensacola, FL,
05/2009 - 12/2010

Publications:

“Event-by-Event Simulations of Jet Modification Using the MATTER Event Generator”
Hard Probes 2016 Proceedings

“Jets in $d(p)$ -A Collisions: Color Transparency or Energy Conservation” In Progress

“Jets and Centrality in $p(d)$ -A Collisions” Hard Probes 2015 Proceedings